Design and Analysis of a High Speed Smart Materials Based Nano-Positioner

Ismail Shujau

A thesis submitted in partial fulfilment of the requirements for the Degree of

Master of Mechanical Engineering

Department of Mechanical Engineering

University of Canterbury

Canterbury

New Zealand

31st of March, 2005

بسم الله الرحمن الرحيم

"In the name Allah, Most Gracious, Most Merciful"

"All praise to Allah, the Lord of the Worlds, Creator of the entire universe, the One and only."

Peace and blessing to our beloved prophet Muhammad (s.a.w.), his family, companions and those who follow him

Abstract

Nanometre accuracy is required by many modern microactuators to provide the accuracy and small motions necessary for micro-assembly and nano-lithography. Piezoelectric actuators are designed to do just that, and are now possible to get displacements in the order of picometre range. Combined with high stiffness, fast frequency response and high bandwidth, they are ideal for precision positioning applications

The present work is based on work of Goldfarb and Celanovic [3]. A single layer and a multilayer piezoelectric actuator model are developed, with PID closed-loop feedback control to control each layer in piezoelectric stack separately, to achieve the commanded displacement profiles. The models are simulated in MATLAB. In each case, the results show fast response times of 0.3 milliseconds or less. Multilayer model is able to control individual layers separately or all simultaneously, with similar or better response times. In each case, the model showed the ability to track displacements ranging from 1 nm to several μm.

Acknowledgements

I would like to thank Associate Professor Geoffrey Chase and Dr. Chris Hann for their supervision, helpful guidance, useful discussions and valuable feedback. I would also like to thank my parents, my wife and daughter for their constant support and motivation. Finally, I would like to thank all my friends for their help in this home away from home.

Contents

Chapter 1 **1**

1 Introduction 1

1.1 Piezoelectric Materials and Actuators 3

1.2.1 Types of PZT actuators 4

1.2 Modelling and Prior Art 10

1.3 Research Objectives 16

1.4 Organisation 17

Chapter 2 **19**

2. Model Realization 19

2.1 Single Layer Model 19

2.2 Modelling Hysteresis 20

2.3 Multilayer Model 24

2.4 Simulation Method 25

2.4.1 Single layer PZT actuator 25

2.4.2 Multilayer PZT actuator 25

Chapter 3 **27**

3 Single Layer Simulation 27

3.1 Hysteresis with One Elasto-Slide Element 28

3.2 Hysteresis with Multiple Elasto-Slide Elements 29

3.2.1 Closed loop PID control 34

3.3 Simplified Model 39

Chapter 4 **42**

4 Multilayer Analysis 42

4.1 Simulation of Multilayer PZT Actuator 43

Chapter 5 **53**

5 Conclusions and Future Work 53

References **56**

Appendices **58**

List of Figures

Figure 1.1	Configuration of a PZT one layer stack.	4
Figure 1.2	Free PZT layer and an electrically activated bimorph [10].	5
Figure 1.3	Serial PZT bimorph actuator [9, 10].	6
Figure 1.4	Parallel PZT bimorph actuator with middle electrode [9, 10].	6
Figure 1.5	PZT stack actuator [9]	7
Figure 1.6	Bare stack actuator [10].	8
Figure 1.7	Typical ring actuators and a schematic diagram [10].	9
Figure 1.8	Stack actuator with pre-load and a schematic showing internal structures [10].	10
Figure 1.9	Block diagram of position control system based on PID and feedback linearization [7].	13
Figure 1.10	Principle of inertial drive or stick-slip model [4].	15
Figure 2.1	Schematic representation of the PZT stack actuator model [3, 13].	19
Figure 2.2	Experimental observations by [3], measured quasi-static relations between applied voltage and endpoint displacement, and applied force and endpoint displacement.	21
Figure 2.3	Single elasto-slide element consisting of a massless linear spring and a massless block subjected to Coulomb friction and its force-displacement behaviour, taken from [3].	22
Figure 2.4	Schematic of a system with n elasto-slide elements in parallel, and its force-displacement behaviour, taken from [3].	24
Figure 2.5	Multilayer PZT stack.	24
Figure 3.1	Force-displacement behaviour of a single layer with one elasto-slide element.	29

Figure 3.2 Force-displacement behaviour for a multiple (ten) elasto-slide element model. 30

Figure 3.3 Output displacement and voltage-displacement behaviour for a ten elasto-slide element PZT actuator with a 60 volt steady sinusoidal input voltage. 31

Figure 3.4 Output displacement and voltage-displacement behaviour for a ten elasto-slide element PZT actuator with a 90 volt decaying sinusoidal input voltage. 32

Figure 3.5 Output displacement and voltage-displacement behaviour for a ten elasto-slide element PZT actuator with a 90 volt steady triangular input voltage. 33

Figure 3.6 Voltage-displacement behaviour for a ten elasto-slide element PZT actuator with a 30,60, and 90 volt steady triangular input voltage. 34

Figure 3.7 Output displacements for different reference inputs showing the range, from 1 nm to 12 μm. 36

Figure 3.8 Output displacements for different reference inputs with an external force of 1 Newton. 37

Figure 3.9 Output displacements for different reference inputs with an external force applied after steady state. 38

Figure 3.10 Displacement behaviour of the PZT for Triangular input, for full model (including mass of PZT) and simplified model (excluding mass). 39

Figure 3.11 Voltage versus displacement behaviour of the PZT for Triangular input, for full model (including mass of PZT) and simplified model (excluding mass). 40

Figure 4.1 Schematic model of a 3 layer PZT actuator. 42

Figure 4.2 Displacement behaviour for a 90 volt, 100 Hz, triangular wave applied to all three layers. 44

Figure 4.3	Displacement behaviour for only layer 1 activated.	44
Figure 4.4	Displacement behaviour for only layer 2 activated.	45
Figure 4.5	Displacement behaviour for 1 nm reference input.	46
Figure 4.6	Displacement behaviour for 10 nm reference input.	46
Figure 4.7	Displacement behaviour for 12 μm reference input.	47
Figure 4.8	Displacement behaviour for 1, 5, and 10 nm reference input to 3 layers.	48
Figure 4.9	Input displacement command profile for three layer actuation.	49
Figure 4.10	Endpoint output displacement behaviour of PZT actuator for input displacement profile shown in Figure 4.9	50
Figure 4.11	Endpoint output displacement behaviour of PZT actuator for 1 nm step inputs at each layer.	50

List of Tables

Table 3.1 Generalised Maxwell Capacitor parameters utilised in the model, taken from [3]. 27

Table 3.2 Model parameters utilised in simulation, taken from [3]. 28

Chapter 1

1. Introduction

Piezoelectric actuators (PEA) are used as precision microactuators for micropositioning devices and are especially useful in dynamically interactive micromanipulation applications. PEA can deliver up to the order of picometre (1 pm = 10^{-12} m) accuracy in position tracking performance in addition to robustly stable force control [1]. Combined with high stiffness, fast frequency response [2], no significant mechanical backlash and, high bandwidth [3], make PEAs ideal for precision positioning applications.

There are many advantages of using PEA over the traditional mechanical or electro-mechanical actuators and these include:

- High resolution – PEA can produce smooth subnanometer level changes in displacement [1, 4].
- Large force generation – PEAs can generate large forces [4, 5].
- Fast expansion – PEAs offer extremely fast response times on the order of milliseconds or less [4].

- No magnetic fields – Since piezoelectric effect is only related to electric field, they don't produce unnecessary magnetic fields. This feature is very favourable where magnetic fields cannot be tolerated [4].
- No wear and tear – PEAs have no moving parts hence no wear [4].
- Low power consumption – Energy is absorbed only in movements, while static operations like holding do not consume power [4].
- Vacuum and clean room compatible – Since PEAs do not need lubrication they are ideal for ultra high vacuum applications commonly found in microfabrication of silicon chips [4].

These benefits make PEA suitable for a number of applications. The growing need and versatility of PEA can be envisaged by glancing at the wide range of applications of these actuators. Some of these applications include advanced microlithography [6], scanning microscopy [2, 4, 7], automated microassembly, precision machining [8], microsurgery [7], vibration and buckling control, tool adjustments, micro pumps, needle valve actuation, nano-metrology, and shockwave generation [4]. The versatility of this smart material is also being explored for other areas as well.

A disadvantage of PEA is hysteresis behaviour, giving rise to a highly nonlinear output displacement response to a given voltage input. Control of PEA is greatly facilitated by model-based control system analysis and design. This research concentrates on understanding and implementing previous nonlinear models of PEA that account for

hysteresis and to extend to a multi-layer PEA where each layer is controlled separately, thus giving smaller displacements, increasing bandwidth and increasing force generation. Extension to a multilayer PEA will include the reformulation of the nonlinear dynamics of hysteresis to an easily implementable form that is suitable for model-based controller design.

1.1 Piezoelectric Materials and Actuators

The property of peizoelectric materials that gives rise to this very useful and unique behaviour is called the piezoelectric effect. In 1880 the Curie brothers discovered that pressure applied to a quartz crystal created an electric charge in the crystal. They called this electro-mechanical behaviour piezo effect, derived from the Greek word for pressure [9].

A piezoelectric material transfers energy between electrical and mechanical domains [3]. In uncomplicated terms this relationship means a voltage applied to a piezoelectric material induces a mechanical strain on it surfaces, and a strain applied to a piezoelectric material induces a voltage across its surface. The latter effect is known as the piezoelectric effect and the former effect is the inverse piezoelectric effect, and is also the basis of a PEA.

Naturally occurring piezoelectric materials like quartz are of limited use in these applications, because their piezoelectric properties are too small for practical use [1].

On the other hand, synthetic piezoelectric materials like lead-zirconate-titanate (PZT) are more appropriate for such applications and can generate significant forces. Such a PZT one layer actuator is shown in Figure 1.1, using a single material layer. In Figure 1.1 a voltage difference between the electrodes, ΔV, creates a material strain and thus motion and/or force.

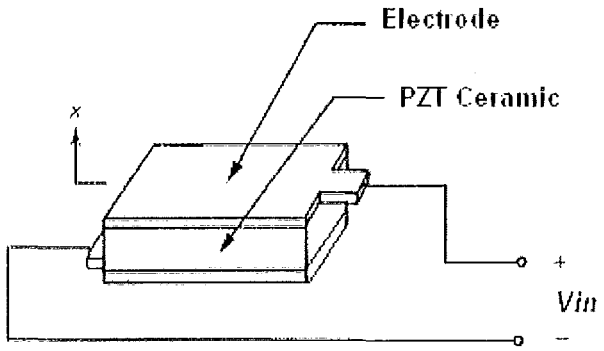

FIGURE 1.1: CONFIGURATION OF A PZT ONE LAYER STACK

Synthetic PZT is polarised in one direction and exhibits significant piezoelectric effect in this direction [3]. Although the elongation produced by this material is relatively small, they can develop large forces quite rapidly [5]. A typical PZT actuator can generate only 1-2 μm of displacement before fracture. However, due to large Young's modulus of 5-6 MPa, the resulting tractions or forces can be very large.

1.2.1 Types of PZT actuators

Basically there are three types of PZT actuators: bimorphs, stacks and tubes. Typical PZT stack actuators use variation in the PZT thickness as the displacement mechanism. Bimorphs (or bending actuators), on the other hand use the planar

motion that accompanies the bending moments they generate over the two layers. Similar to the action of thermo-bimetals, PZT bimorphs induces a mechanical stress due to the planar motion when electrically activated [10]. This motion results in a bending movement of the PZT bimorph as shown in Figure 1.2.

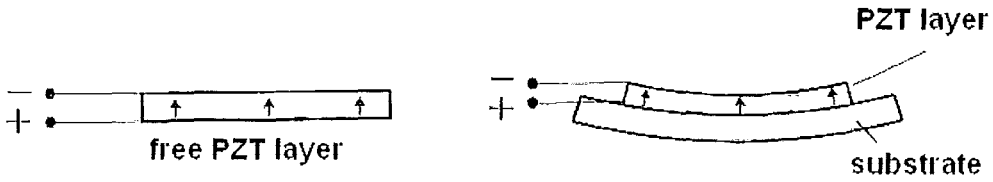

FIGURE 1.2: FREE PZT LAYER AND AN ELECTRICALLY ACTIVATED BIMORPH [10]

Advantages of using PZT bimorphs include:

- Larger travels than PZT stack actuators for comparable operating voltages [10]. Hence, they can generate more motion for similar or lesser force
- Simple structure
- Flat design
- Wider range of operating parameters
- Consumes less power [4]

There are three types of PZT bimorphs and they are serial, parallel and multilayer benders or bimorphs. Serial bimorphs consist of two thin PZT layers with opposing polarisation that are glued together. Electrodes are then placed on both surfaces as shown in Figure 1.3. An application of voltage leads to contraction of the PZT layer,

where the electric field and polarisation are parallel, and expansion of PZT layer where the electric field and the polarisation are anti parallel, thus producing the bending motion.

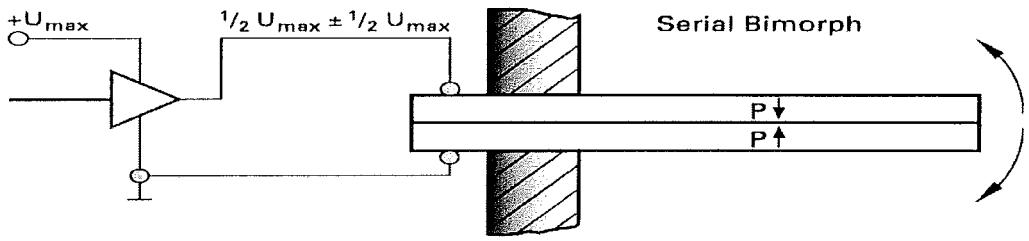

FIGURE 1.3: SERIAL PZT BIMORPH ACTUATOR [9, 10]

Parallel benders have two thin PZT layers with same polarisation direction and three electrodes, two surface electrodes and one middle electrode as shown in Figure 1.4. The middle electrode, usually a metal sheet improves the mechanical properties of the bender. Also having an extra electrode gives the parallel bimorph more alternatives for driving modes than the serial bimorph.

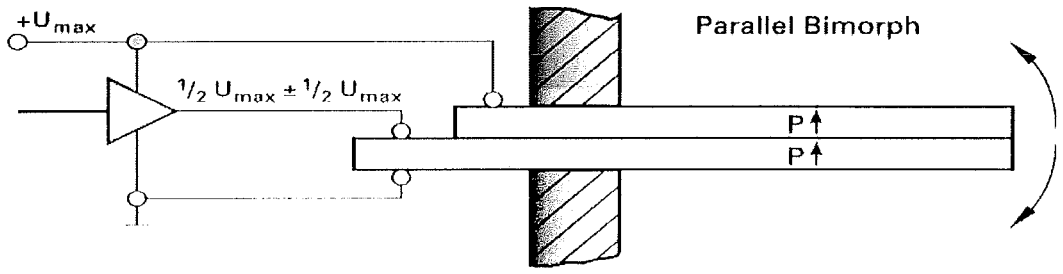

FIGURE 1.4: PARALLEL PZT BIMORPH ACTUATOR WITH MIDDLE ELECTRODE [9, 10]

Multilayer benders are similar to parallel benders with three electrical connections but are built with more than two PZT layers. The layers in a multilayer bender are joined together by high temperature sintering (rather than adhesive) [10]

On the other hand, stack actuators use variation in the PZT thickness as the displacement. There are three types of stack actuators which include bare stacks, ring stacks and cased stacks with internal preload mechanisms. Stacks are made of several PZT layers stacked on top of each other with electrodes between each PZT layer. The PZT layers are mechanically in series but are electrically in parallel as shown in Figure 1.5.

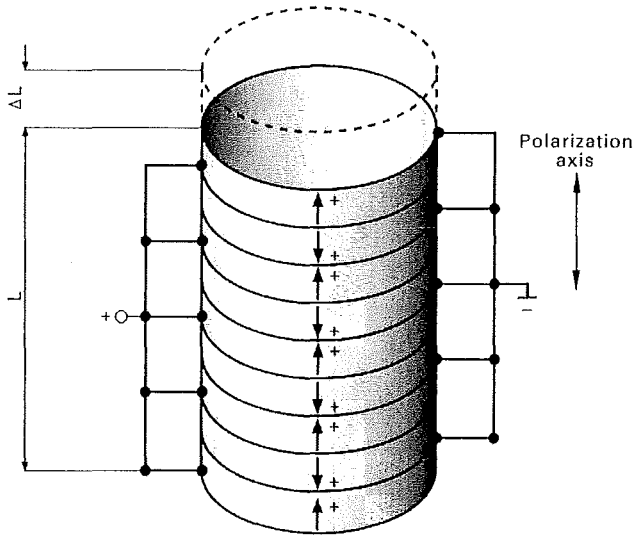

FIGURE 1.5: PZT STACK ACTUATOR [9]

Bare stacks, shown in Figure 1.6, consist of ceramic disks separated by thin metallic electrodes so that the sides face show +/- alternating electrodes that can be connected to electric wires. The bare electrodes are a critical point for corrosion and must be

appropriately coated for acceptable reliability and lifetime [10]. The most common coating is ceramic. In addition to this coating, platinum internal electrodes are used to give the highest electrical and electro-chemical stability. Of all type of actuators, stack actuators show the highest stiffness and can withstand high pressures. Because of the high stiffness they can also generate large forces. Finally, while each stack layer exhibits very small motion, the total stack can offer large motion. The only drawback is that as stacks grow larger they become more flexible, which can impact precision.

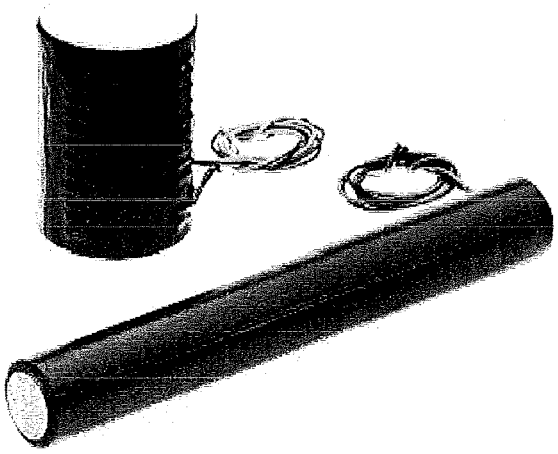

FIGURE 1.6: BARE STACK ACTUATORS [10]

Ring actuators are very similar to bare stacks, the only difference being a hole in the middle of the ring actuators. The need for ring actuators is twofold. First is the need for feed through of mechanical parts or transmissive optical setups. The second is to increase the stiffness by enlarging the diameter without increasing the volume of actuator. Furthermore, ring actuators provide better cooling for high frequency or

high voltage applications due to access of both inner and outer surface for coolant [10]. Typical ring actuators are shown in Figure 1.7.

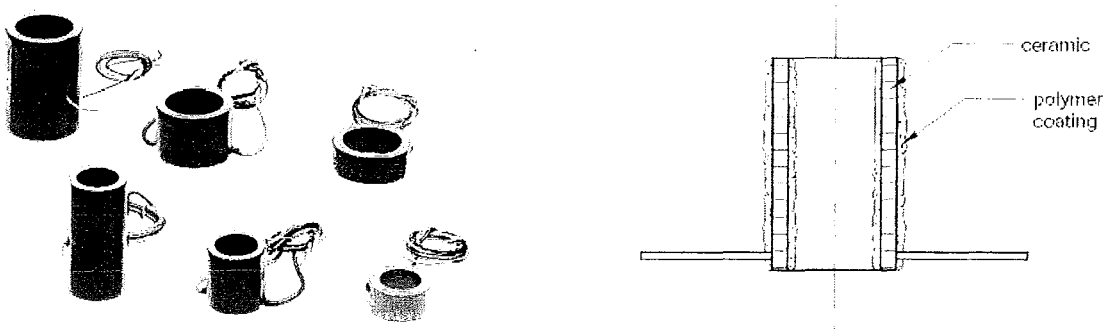

FIGURE 1.7: TYPICAL RING ACTUATORS AND A SCHEMATIC DIAGRAM [10]

Finally both ring and stack type actuators can be modified to include a casing and a preload or a pre-stress. This pre-load is typically achieved by some kind of spring mechanism. The main reason for pre-stressed actuators is to get a more symmetrical push/pull performance. It is a widely accepted that PZT ceramics, though outstanding in producing high pushing force, are poor in generating tensile force. To overcome this drawback a resetting force is incorporated into the actuator. Figure 1.8 shows a diagram of a stack actuator with pre-stress mechanism.

PZT actuators can also be classified by their operating voltages. Under this classification there are two types of PZT actuators; low voltage actuators and high voltage actuators. The low voltage PZT actuator needs about 100 volts to get the maximum displacement, while the high voltage actuator can operate up to 1000 volts.

These high voltage actuators have a higher operating temperature of up to 150^0 Celsius, compared to 80^0 Celsius for low voltage PZT.

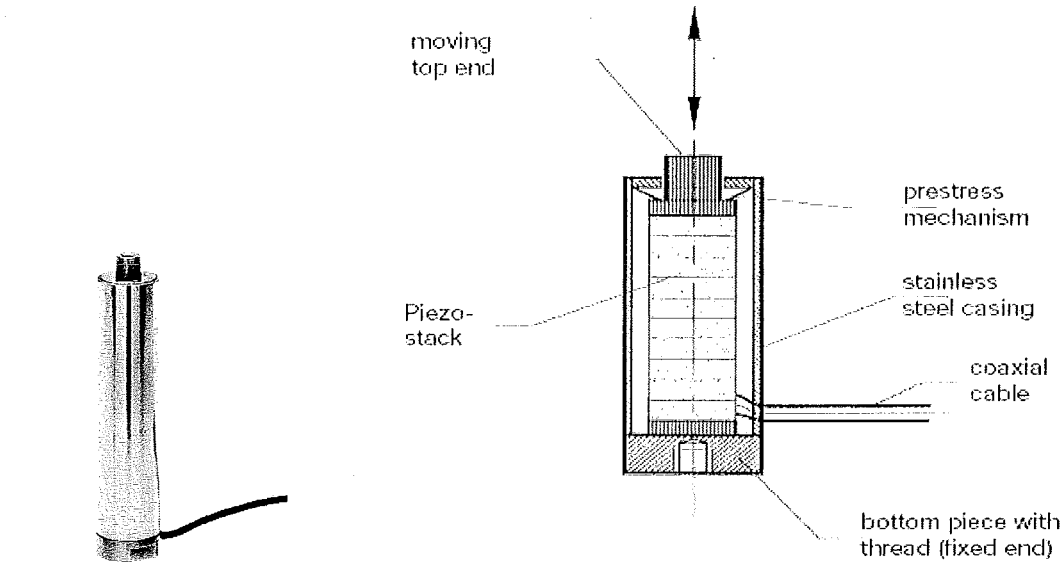

FIGURE 1.8: STACK ACTUATOR WITH PRELOAD AND A SCHEMATIC DIAGRAM SHOWING INTERNAL STRUCTURES [10]

1.2 Modelling and Prior Art

One of the major limitations of piezoelectric actuators is lack of accuracy due to material hysteresis and drift. The most widely recognised description was published by standards committee of the IEEE which only looks into linear constitutive relations. This is typically represented in compressed matrix notation as follows [3]:

$$S_p = s^E_{pq} T + d_{kp} E_k \tag{1.1}$$

$$D_i = d_{iq} T_q + \varepsilon^T_{ik} E_k \tag{1.2}$$

Where S represents the strain tensor, s^E is the elastic compliance matrix when subjected to a constant electrical field, T represents the stress tensor, d is a matrix of piezoelectric material constants, E is the electrical field vector, D is the electric displacement vector, and $\varepsilon^T$is the permittivity measured at a constant stress. However, this description fails to address the hysteresis nonlinearity present in all PEAs [1, 3]. Many prior researches either look at the linear dynamics or nonlinear hysteresis but fail to address both problems together.

One of best descriptions for hysteresis was given by Ge and Jouaneh [2], in which they described that hysteresis is a consequence of domain switching. More specifically, as the applied electric field switches, it does not occur instantaneously. This delayed strain response of the material cause hysteresis. Drift in piezoelectric materials is noticeable in the warm-up transient stage, where material properties and effective electro-mechanical behaviour can vary with time and temperature.

Many efforts have been made to improve the performance degradation due to the hysteretic behaviour of piezoelectric actuators. The most common techniques are:

- Use of electric charge to drive the piezoelectric actuator [1, 11, 12].
- Use of feedforward nonlinear models in driving the actuators [2]
- Use of model-based closed loop control [7, 13]

Newcomb and Flinn [11] proposed the use of charge rather than voltage as the control input so that linear control techniques can be used to control the actuator. They found that if the output displacement is plotted against the applied charge, rather than the voltage, hysteresis virtually disappears. However, a negative aspect of this approach is that it requires a specially designed charge driver.

To improve performance due to hysteresis, Ge and Jouaneh proposed a control technique using feedforward tracking based on classical Preisach PZT model [2]. They used a combination of PID feedback control with hysteresis modelling in the feedforward loop in their model. The control output for this controller was defined:

$$U(k) = K_P\, e(k) + K_I \Sigma e(k) + K_D\,[e(k) - e(k\text{-}1)] + u_h(k) \qquad (1.3)$$

where K_P, K_D and K_I are proportional, differential and integral gains respectively, and $e(k)$ is the error term. The last term, $u_h(k)$, is the feedforward linearization control term which was obtained from a look-up table created in the modelling process [2]. Results using this control scheme showed a maximum error less than 0.45 μm. However, at 450 nm this value is still very large compared to nano-lithography requirements which is around 5-10 μm [6]. Also this model is only valid for tracking cyclic reference signals and does not incorporate the important linear dynamics of the PEA [3].

Choi *et al* [7] developed a similar controller for piezoelectric actuators using a closed loop scheme that incorporates PID control with a linearization loop based on a Maxwell slip model. The goal was to improve precision by mitigating the hysteresis nonlinearity of the PZT actuator. Their PID control algorithm can be written:

$$U(k) = K_P\, e(k) + K_I \Sigma e(k) + K_D/\mathrm{T}\,[e(k) - e(k\text{-}1)] \tag{1.4}$$

where K_P, K_D and K_I are proportional, differential and integral gains respectively, T is the sampling time and $e(k)$ is the error term. Figure 1.9 shows a block diagram of the control scheme based on PID and feedback linearization

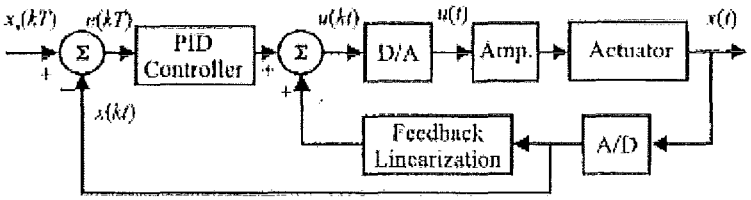

FIGURE 1.9: BLOCK DIAGRAM OF POSITION CONTROL SYSTEM BASED ON PID AND FEEDBACK LINEARIZATION [7]

The dynamic equation of the system for Figure 1.9 was determined from the experimental investigation and is defined:

$$x'' + 193x' + 19600x = 15600f \tag{1.5}$$

where f is the input voltage and x is the position of the actuator. Results show that the error was decreased by 72% using PID with feedback linearization while only 15% of error reduction was achieved with PID only.

Goldfarb and Celanovic [3, 13] also used a Maxwell slip model to describe the hysteresis behaviour. However, the model equations are quite different to that of Choi *et al* [7] and Ge and Jouaneh [2]. The hysteresis is modelled by incorporating an electric element called a Maxwell Resistive Capacitor (MRC – more details of the model and MRC are given in Chapter 2). The behaviour of the actuator was described by the following equations:

$$q = Tx + Cv_t \tag{1.6a}$$

$$v_t = v_{in} + v_{rc} \tag{1.6b}$$

$$v_{rc} = mrc(q) \tag{1.6c}$$

$$mx'' + bx' + kx = F_t + f_{ext} \tag{1.6d}$$

$$F_t = Tv_t \tag{1.6e}$$

where q is the total charge in the PZT stack, v_{in} is the actuator input voltage, v_{rc} is the voltage across the Maxwell capacitor (equivalent to rate independent hysteresis), v_t is the back-emf from the mechanical side, C is the linear capacitance in parallel with the transformer, T is the electromechanical transformer ratio, m, b and k are the mass, damping and stiffness of the PZT stack respectively, x is the stack endpoint

displacement, F_t is the transduced force from the electrical domain, and F_{ext} is the force imposed from the external mechanical load. Equation (1.6c) relates to the voltage across MRC to the charge in the ceramic.

A very different approach is used by Lambert *et al* [8] in which an actuator based on stick-slip effect is realized. This method is also referred as an inertial drive. The basics of stick-slip/inertial method is summarised in Figure 1.10.

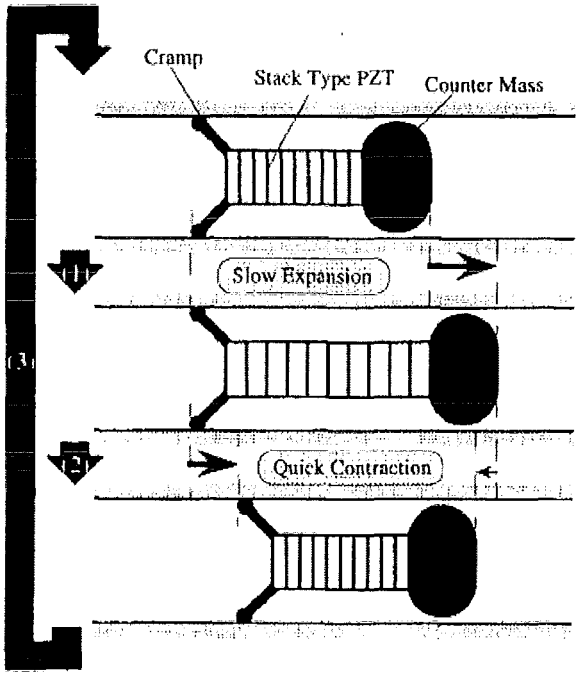

FIGURE 1.10: PRINCIPLE OF INERTIAL DRIVE OR STICK-SLIP METHOD [4].

The stick-slip model shown in Figure 1.10 works in two stages. In the first stage, the actuator slowly translates the carried structure; in the second stage, the legs are moved

back in their initial position very quickly, so that, the inertia gives a displacement in the desired direction [8]. The actuator is most applicable in conveying application.

Finally Kawakita et al [4] have also developed a multi-layered bimorph actuator that employs inertial drive for use in a small maintenance robot for inspection and repairs in cramped and inaccessible locations. Other authors who used this approach include [14, 15].

1.3 Research Objectives

This research will look into the ability to use active control to overcome the tradeoffs in speed, precision and "throw length", limiting high speed nano-positioners. The idea involves individual control of each layer of a PZT stack enabling layers not providing motion to remain stiff, increasing the bandwidth while maintaining precision. This research is based on the modelling work of Goldfarb and Celanovic [3]. It focuses on implementing equations (1.6a) to (1.6e) incorporating PID control to gain active control of the PZT stack to run at 1-2 kHz with a response time of less than 0.5 milliseconds as a result. The reasons for choosing the model developed by Goldfarb and Celanovic for this resaech are:

1. It captures the necessary dynamics of the electromechanical system that we wish to model best.
2. It can be readily implemented and correlated to published work.
3. This model is well accepted in the field.

Specific aims include:

1. Review related literature.
2. Implement the model of Goldfarb and Celanovic for the piezoelectric stack actuator and correlate it with published data.
3. Develop a new actuator control design based on individual layer control in the piezoelectric stack.
    a. Implement model for single layered PZT actuator.
    b. Develop model multi-layered PZT actuator by combining single layered models.
4. Test and verify in simulations

1.4.1 Organisation

Chapter 1 which covers introduction, motivation, general description of PZT actuators, literature review and research goals. Chapter 2 discuses model realization for both single layered and multi-layered PZT actuators. Simulations and model validation for single layered PZT actuators are covered Chapter 3. In Chapter 4 Simulations are done using multi-layered PZT actuator. Chapters 5 discuss conclusions and future work.

Chapter 2

2. Model Realization

2.1 Single Layer Model

Since this study is based on the work of Goldfarb and Celanovic [3, 13], it is appropriate to discuss their work at a deeper level before we proceed. Figure 2.1 shows the electrical and equivalent mechanical model of the PZT actuator used in the model developed by Goldfarb and Celanovic (from here on will be referred as Goldfarb model).

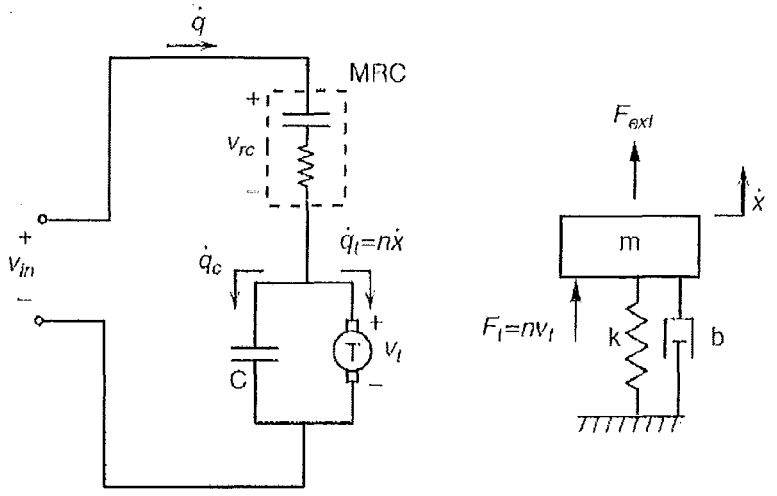

FIGURE 2.1: SCHEMATIC REPRESENTATION OF THE PZT STACK ACTUATOR MODEL [3, 13]

In Figure 2.1, $\dot{q}_c$ is the charge in the parallel capacitor and $\dot{q}_l$ is the charge accumulate the PZT actuator, all the other terms are detailed in section 1.3. The model equations (1.6a) to (1.6e) were stated earlier in section1.3.

Dynamic observation indicates that end-point displacement as a function of electric charge is well approximated by second order dynamics. The rate-independent hysteresis lies solely in the electrical domain, between the applied actuator voltage and resulting charge in the actuator. Thus Equations (1.6a) to (1.6e) link the second order dynamics of end-point displacement with the nonlinear rate-independent hysteresis between the applied actuator voltage and the charge in the actuator.

Equation (1.6a) is perhaps the most important as it describes how the charge in the PZT ceramic relates to both displacement and voltage. It implicitly defines the charge, q, so q is a nonlinear function of displacement, x. Thus the force F_t is a nonlinear function of x, and hence Equation (1.6d) is a nonlinear differential equation that must be solved numerically. Since F_t depends on q, Equation (1.6a) must be solved numerically for q at each time step of any DE solver to determine F_t for the next time step.

2.2 Modelling Hysteresis

Hysteretic behaviour in piezoelectric actuators is a very real and observed effect, and must be modelled to accurately capture the dynamics of any PZT actuated system. Following Goldfarb and Celanovic [3], generalized hysteretic behaviours can be characterised by two variables related by a non-single-valued function as illustrated by the voltage/displacement relationship, (shown in Figure 2.2). In this and in most systems, this hysteretic behaviour is the result of energy storage that is fundamentally coupled to rate-independent dissipation. Mechanically, such behaviour could be modelled by the combination of an ideal spring, which represents pure energy-storage, coupled to a pure Coulomb friction element, which represents rate-independent dissipation. This analogy is the basis for the static hysteresis exhibited by the piezoelectric actuator. Hence, Figure 2.2 (from [3]) illustrates the hysteresis electromechanical dynamics of PZT, which are similar sor any such smart material.

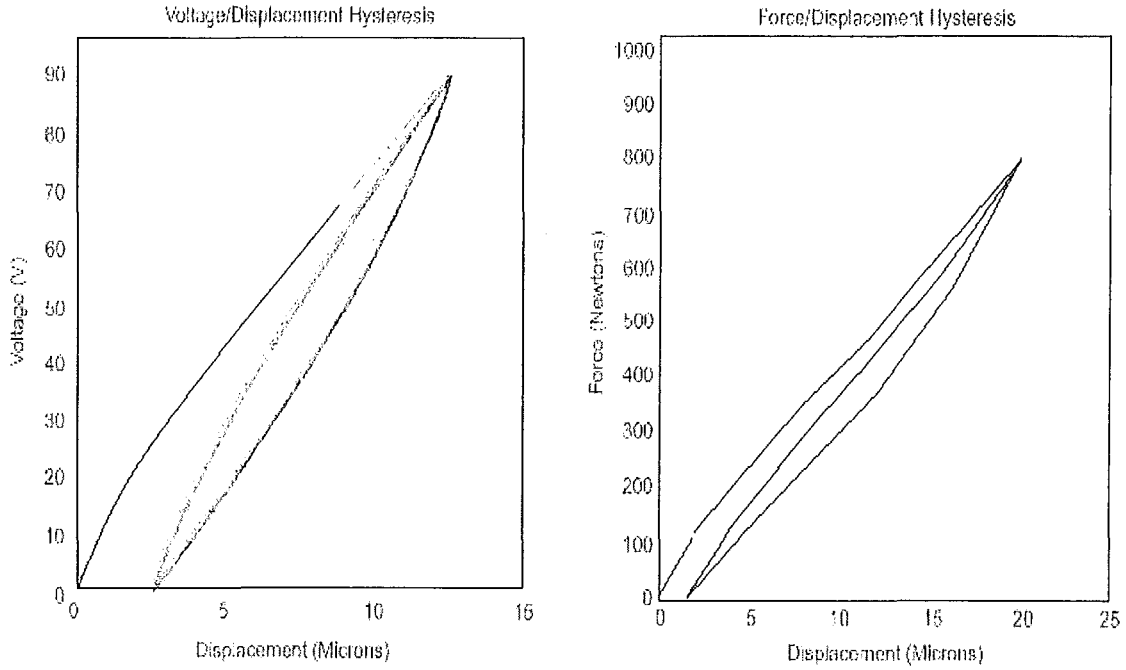

FIGURE 2.2: EXPERIMENTAL OBSERVATIONS BY [3], MEASURED QUASI-STATIC RELATIONS BETWEEN APPLIED VOLTAGE AND ENDPOINT DISPLACEMENT AND BETWEEN APPLIED FORCE AND ENDPOINT DISPLACEMENT

This method for describing hysteretic behaviour can be schematically shown using a single elasto-slide element which is constructed by combining a measles block subject to Coulomb friction and a measles linear spring, as shown in Figure 2.3. The behaviour of this element is defined:

$$F = \begin{cases} k(x - x) \quad if \mid k(x - x_b) \mid < f \\ f\,\mathrm{sgn}(\dot{x}) \; and \; x_b = x - \dfrac{f}{k}\mathrm{sgn}(\dot{x}) \quad else \end{cases} \tag{2.1}$$

where x is the input displacement, F is the output force, k is the stiffness of the spring, $f = \mu N$ is the breakaway friction force of the block, and x_b is the position of the block.

This technique was first constructed by mathematician and physicist James C. Maxwell where instead of one elasto-slide element; the limit is taken with infinite

number of elasto-slide elements. The model is referred as the Generalized Maxwell Slip model [16]. For a system with an arbitrary number of elasto-slide elements, as shown in Figure 2.4, the behaviour can be described by extending Equation (2.1) as follows:

$$F_i = \begin{cases} k_i(x - x_{bi}) \quad if \mid k_i(x - x_{bi}) \mid < f_i \\ f_i \operatorname{sgn}(\dot{x}) \; and \; x_{bi} = x - \dfrac{f_i}{k_i}\operatorname{sgn}(\dot{x}) \quad else \end{cases} \tag{2.2}$$

$$F = \sum_{i=1}^{n} F_i \tag{2.3}$$

where x is the input displacement, F is the total output force, $F_i, k_i, f_i, and\ x_{bi}$ are the output force, spring stiffness, breakaway force and block position, respectively, of I^{th} elasto-slide element.

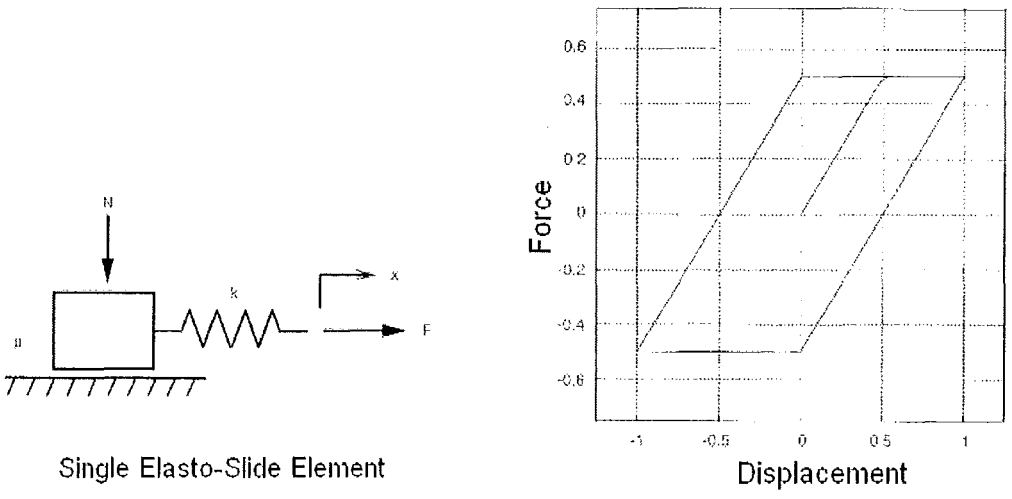

FIGURE 2.3: SINGLE ELASTO-SLIDE ELEMENT CONSISTING OF A MASSLESS LINEAR SPRING AND A MASSLESS BLOCK SUBJECTED TO COULOMB FRICTION AND ITS FORCE-DISPLACEMENT BEHAVIOR TAKEN FROM [3].

As stated in [3], the generalised Maxwell Resistive Capacitance, indicated as MRC in Figure 2.1, resides in the electrical domain and therefore relates the element's electrical voltage across the MRC to the charge in the ceramic. The voltage across the MRC is defined:

$$V_i = \begin{cases} \dfrac{(q - q_{bi})}{C_i} & if \quad |\dfrac{(q - q_{bi})}{C_i}| < v_i \\ v_i \operatorname{sgn}(\dot{q}) & and \quad q_{bi} = C_i v_i \operatorname{sgn}(\dot{q}) \quad else \end{cases} \tag{2.4}$$

$$v_{rc} = \sum_{i=1}^{n} V_i \tag{2.5}$$

where q is the charge in the ceramic, v_{rc} is the voltage across the Maxwell capacitor, and all other variables are the electrical analogues of those in Equations (2.2) and (2.3) given by $k_i = \dfrac{1}{C_i}$ and $v_i = f_i$.

In comparison to Figure 2.3, Figure 2.4 shows a smooth curve for displacement-force behaviour. This is because in Figure 2.3 only one elasto-slide element is used. As the number of elasto-slide elements increase the model becomes more accurate and the displacement-force curve becomes smoother. This is evident in Figure 2.4 where ten elasto-slide elements are used.

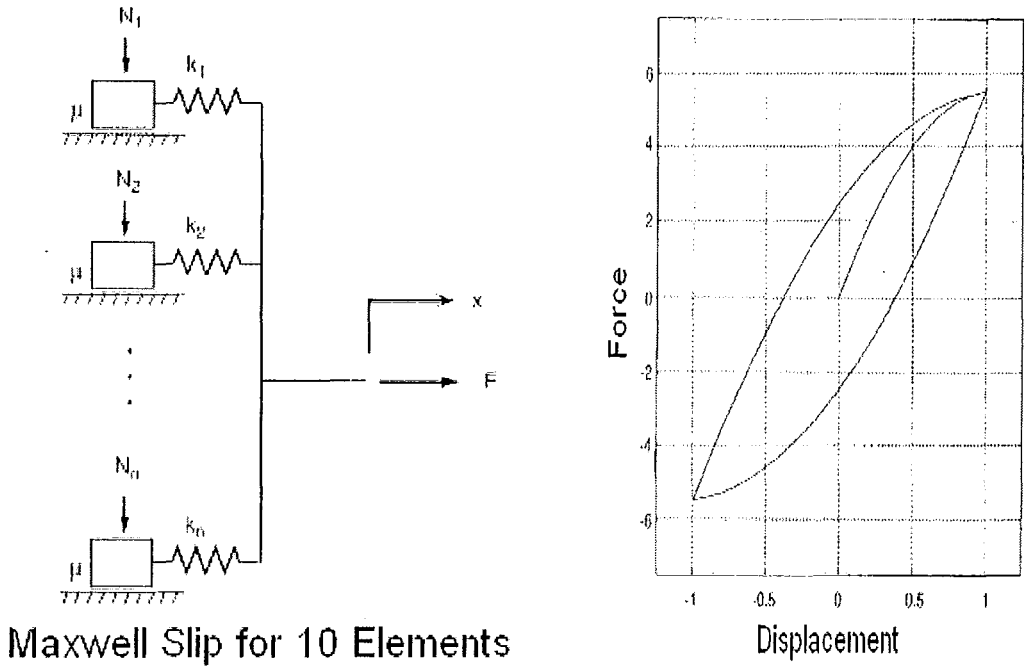

FIGURE 2.4: SCHEMATIC OF A SYSTEM WITH *n* ELASTO-SLIDE ELEMENTS IN PARALLEL, AND ITS FORCE-DISPLACEMENT BEHAVOUR, TAKEN FROM [3]

2.3 Multilayer Model

A multilayer PZT stack model is developed by cascading the basic PZT single layer model. A multilayer PZT stack with three layers is developed in which each layer is control individually or all of them are controlled altogether. The important thing to consider is the interactive forces and strains that come into action between layers, especially when a given layer is not activated. For example in a there layer stack, as shown in Figure 2.4, if only layer PZT2 (middle layer) only stretches there will be an induced pulling force on PZT1 and a pushing force on PZT3.

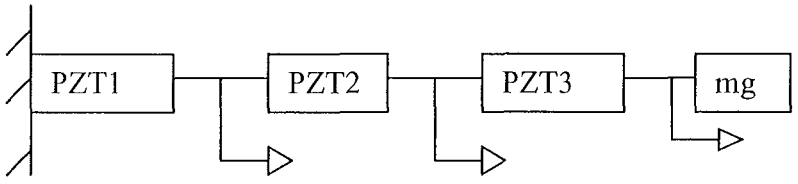

FIGURE 2.5: MULTILAYER PZT STACK

If we assume that the mechanical properties of each PZT layer are the same, the dynamics of the system can be expressed in matrix notation as follows:

$$\begin{bmatrix} m_1 & 0 & 0 \\ 0 & m_2 & \\ 0 & 0 & m_3 \end{bmatrix} \begin{Bmatrix} \ddot{x}_1 \\ \ddot{x}_2 \\ \ddot{x}_3 \end{Bmatrix} + \begin{bmatrix} 2b & -b & 0 \\ -b & 2b & -b \\ 0 & -b & b \end{bmatrix} + \begin{Bmatrix} \dot{x}_1 \\ \dot{x}_2 \\ \dot{x}_3 \end{Bmatrix} + \begin{bmatrix} 2k & -k & 0 \\ -k & 2k & -k \\ 0 & -k & k \end{bmatrix} \begin{Bmatrix} x_1 \\ x_2 \\ x_3 \end{Bmatrix} = \begin{Bmatrix} F_{t1} \\ F_{t2} \\ F_{t3} \end{Bmatrix} \tag{2.6}$$

where m_1, m_2 and m_3 are the masses of the PZT ceramics, b is the damping constant, k is the spring constant, and x_1, x_2 and x_3 are the displacements in each layer. It will be shown in single layer PZT actuator analysis that the mass of the PZT ceramic has negligible effect on the total performance, hence will be omitted in the model for multilayer PZT actuator, reducing the system to first-order matrix system.

The hysteresis nonlinearity is still defined by Equations (1.6a), (2.4) and (2.5), where v_{rc} is calculated for every time step for each layer.

2.4 Simulation Method

2.4.1 Single layer PZT Actuator

The solution to this system lies in solving the system defined in Equation (1.6a) to (1.6e) that describes a single layer PZT actuator. This task is achieved using Euler's method with a very small time step size to ensure stability and following the following four steps:

1. Solve Equation (1.6a) for q, assume initial conditions are zero
2. Find v_{rc} using q and utilising Equations (2.4) and (2.5)
3. Get F_t by substituting in Equations (1.6b) and (1.6e)

4. Solve Equation (1.6d) for x using Euler's method.

In tackling this problem, first the above mentioned method is applied to a single layer with only one elasto-slide element. This is then extended to a ten elasto-slide element to one PZT layer. Closed loop control is then attained by apply PID control.

2.4.2 Multilayer PZT Actuator

As expected multilayer PZT actuator is simulated by putting the single layers together and relating the inter-layer forces by Equation (2.6).

Chapter 3

3. Single Layer Simulation

The model is developed in Chapter 2 is simulated using MATLAB. The Maxwell capacitor parameters, which are required to utilise in the Equation (2.4), are taken from Goldfarb and Celanovic's [3] work and are shown in Table 3.1. The other model parameters are shown in Table 3.2.

TABLE 3.1: GENERALISED MAXWELL CAPACITOR PARAMETERS UTILISED IN THE MODEL TAKEM FROM [3]

Element	Stiffness	Break Force
i	Ki (1/Ci)	fi (vi)
1	2.0	0.2
2	0.6	0.3
3	0.3	0.3
4	0.26	2.6
5	0.06	0.9
6	0.1	2.0
7	0.05	1.5
8	0.03	1.2
9	0.1	7.0
10	0.5	80.0

TABLE 3.2: MODEL PARAMETERS UTILISED IN SIMULATION, TAKEN FROM [3].

Model Parameter	Symbol	Numerical Value
Mass	m	0.00375 kg
Stiffness	k	6×10^6 N/m
Damping	b	150 N-s/m
Linear Capacitance	C	1.2×10^{-6} F
Transformer Ratio	T	10 C/m

These parameter values were originally determined by a piecewise linear fit of the measured voltage versus charge data by the authors [3].

The MATLAB program is developed in several stages. First, only one elasto-slide element is modelled. Then the model is developed to accommodate multiple elasto-slide elements as a part of a single PZT layer. PID control for single layer PZT actuator is implemented next. Finally, PID control is applied for a multiple layer model of a PZT stack with multiple elasto-slide elements per layer.

3.1 Hysteresis with One Elasto-Slide Element Model

The single layer with one elasto-slide element is the simplest model possible. Hence, it is a good starting point for modelling and verification. This model consist of a single layer of PZT and the hysteresis behaviour is modelled by only one elasto-slide element as shown in Figure 2.3. The results for this model are shown in Figure 3.1, which shows force-displacement behaviour for this model. Comparing Figure 3.1 to Figure 2.3 it is evident the results are the same, verifying the model. Note that the

hard corners in Figures 2.3 and 3.1 are due to using a single elasto-slide element to capture the hysteretic behaviour.

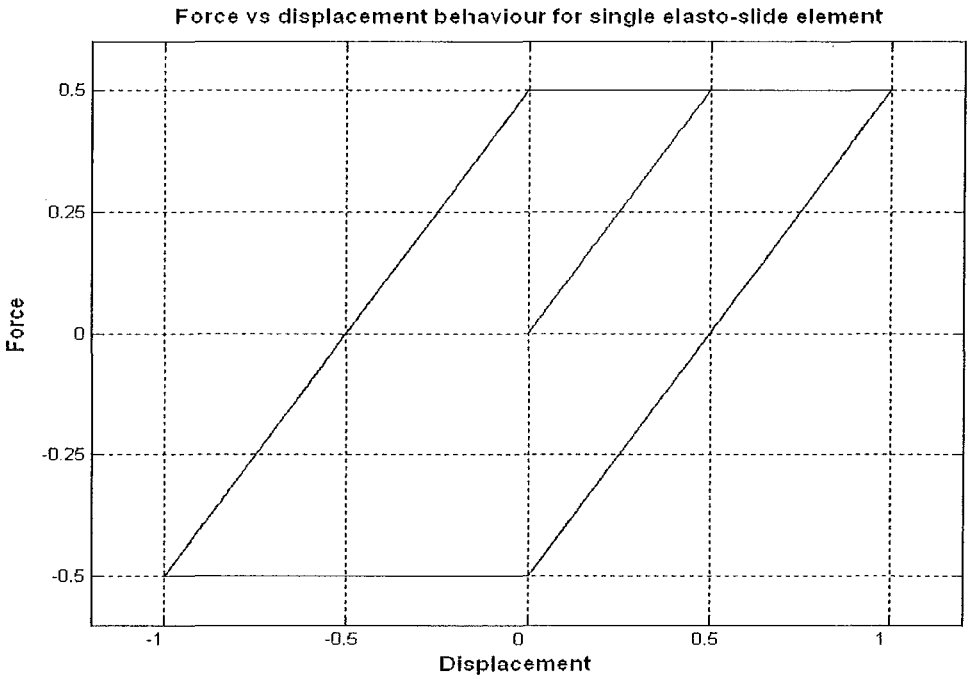

FIGURE 3.1: FORCE-DISPLACEMENT BEHAVIOUR OF A SINGLE LAYER PZT WITH ONE ELAST-SLIDE ELEMENT.

3.2 Hysteresis with Multiple Elasto-Slide Elements

To accurately model hysteresis in a PZT actuator, more than one elasto-slide element is required. Hence, a model with ten elasto-slide elements for each layer of PZT stack was formulated. General force-displacement behaviour is simulated using a sine wave input, and the result is shown in Figure 3.2. This result matches the findings of Goldfarb and Celanovic [3], which are also shown in Figure 2.4. Note that the increased number of nonlinear elasto-slide elements in series provides a better, smoother approximation to observed experimental results.

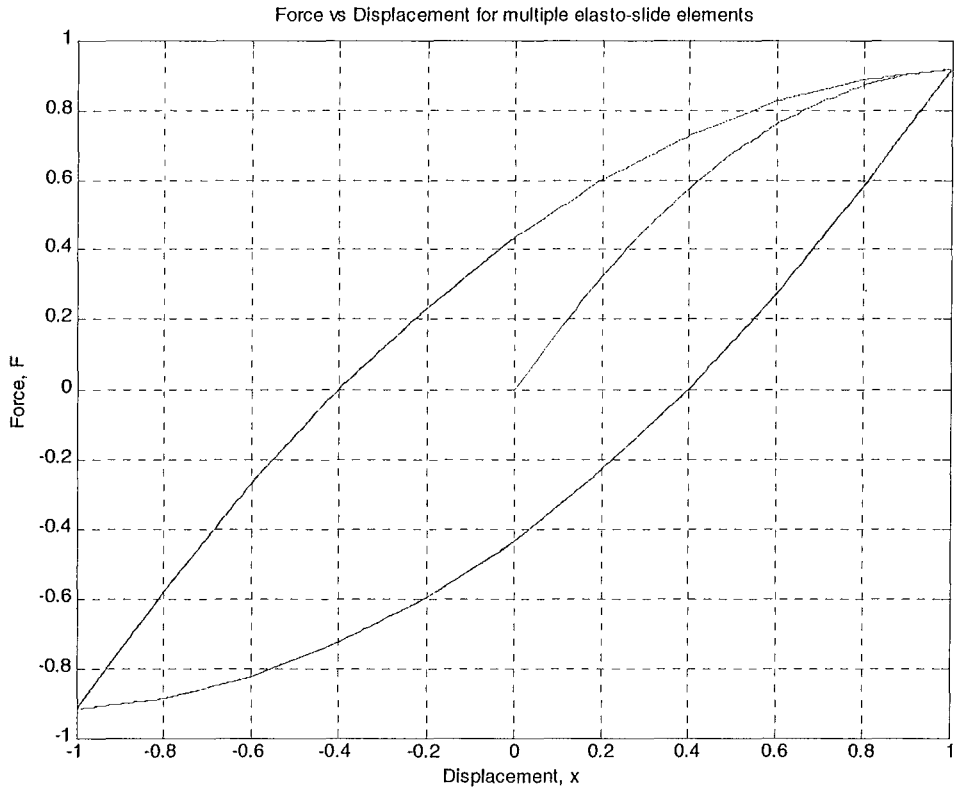

FIGURE 3.2: FORCE-DISPLACEMENT BEHAVIOUR FOR A MULTIPLE (TEN) ELASTO-SLIDE ELEMENT MODEL

The model is then tested with different types of input voltage profiles, specifically; steady, decaying sinusoidal and triangular wave forms are used to test the model. Simulation results are shown in Figures 3.3 to 3.6. In each case, the results match the findings of Goldfarb and Celanovic [3], further validating the model and software.

Figures 3.3 shows the displacement output for a steady sinusoidal input, Figure 3.4 shows the displacement output for a decaying sinusoidal input and Figure 3.5 shows the displacement output for a steady triangular input. The distortion on both the rising and falling slopes and the distinct discontinuities present at the two extremes of motion shows the presence of rate-independent hysteresis in the PZT actuator [3].

Figure 3.6 shows the voltage versus displacement for 90, 60, and 30 volt, 100 Hertz, triangular wave voltage inputs, which can easily be compared to the findings of [3]. It is fair to say that the model accurately represents the behaviour of PZT actuator and models hysteresis nonlinearity as expected. More specifically, as the peak voltage increases the rate at which it rises also increases to match the 100 Hz input frequency. Note that the net slope of the hysteresis loops decreases as the voltage rises. However, the hysteresis loops grow wider capturing the additional energy absorbed by driving the PZT layer at a higher rate. This result is due to material structural damping that is rate dependent.

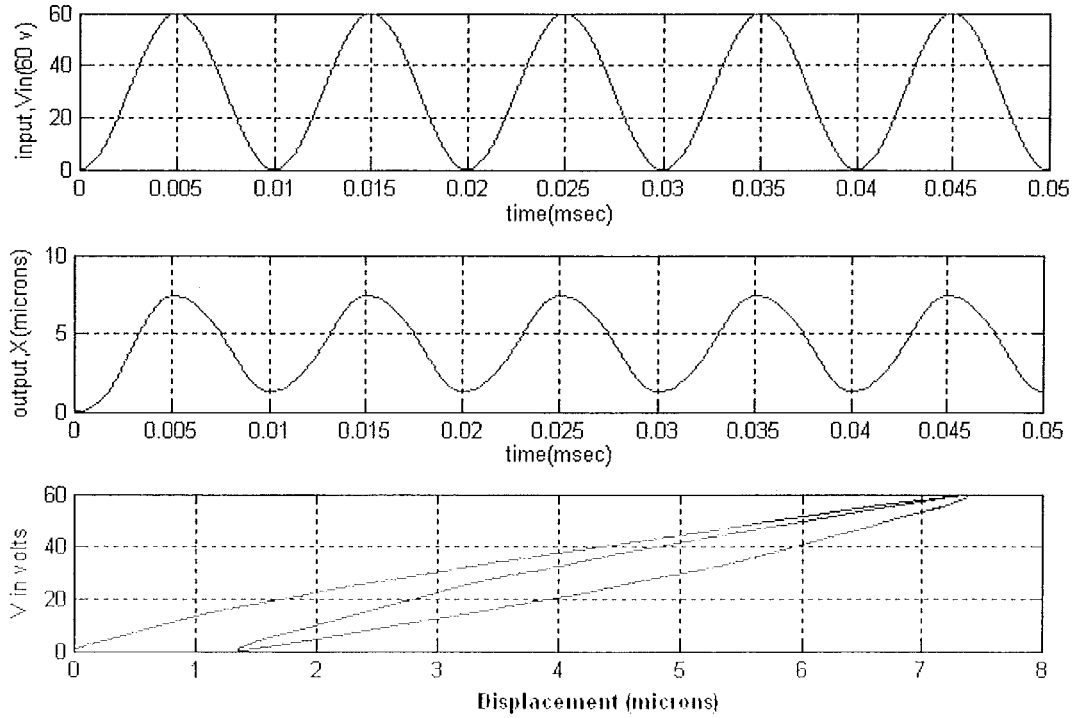

FIGURE 3.3: OUTPUT DISPLACEMENT AND VOLTAGE DISPLACEMENT BEHAVIOUR FOR A TEN ELASTO-SLIDE ELEMENT PZT ACTUATOR WITH A 60 VOLT STEADY SINUSOIDAL INPUT VOLTAGE.

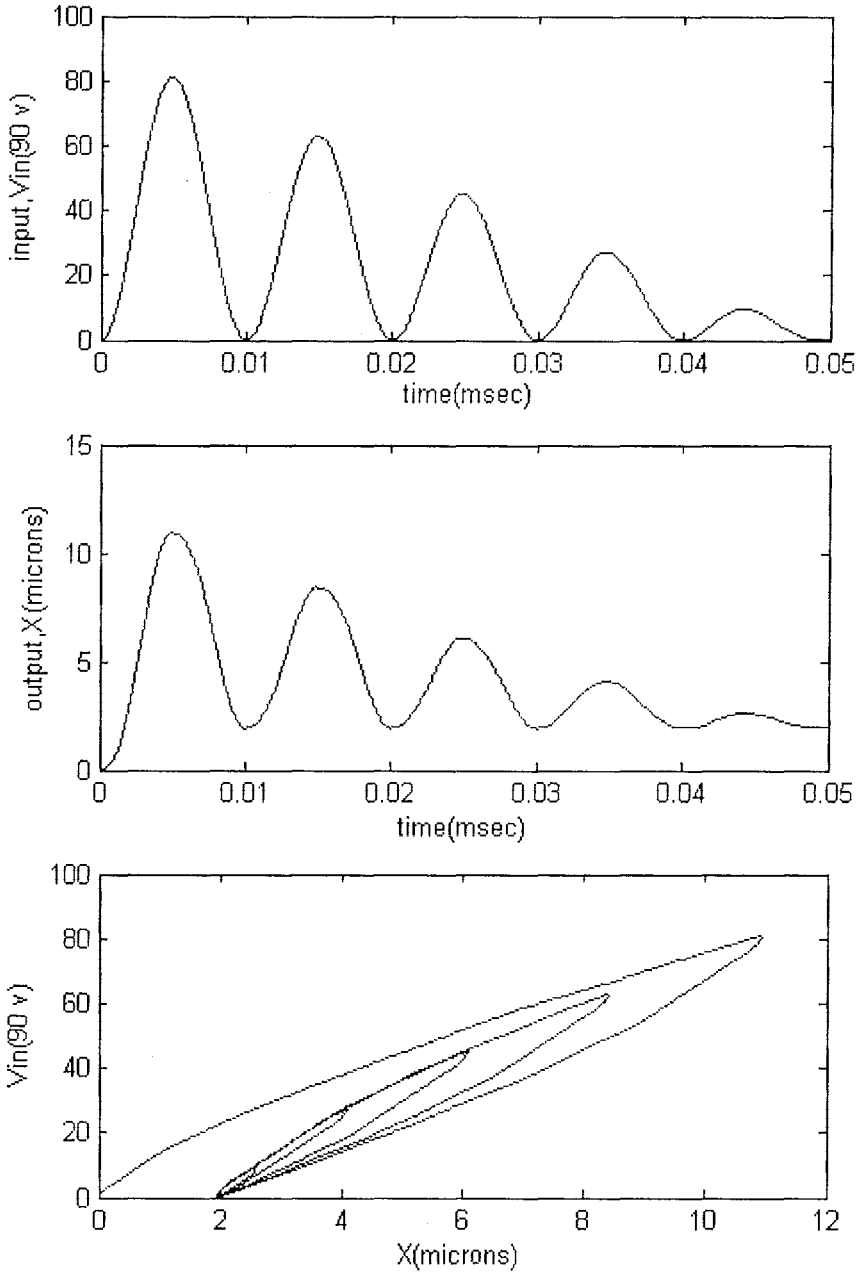

FIGURE 3.4: OUTPUT DISPLACEMENT AND VOLTAGE DISPLACEMENT BEHAVIOUR FOR A TEN ELASTO-SLIDE ELEMENT PZT ACTUATOR WITH A 90 VOLT DECAYING SINUSOIDAL INPUT VOLTAGE.

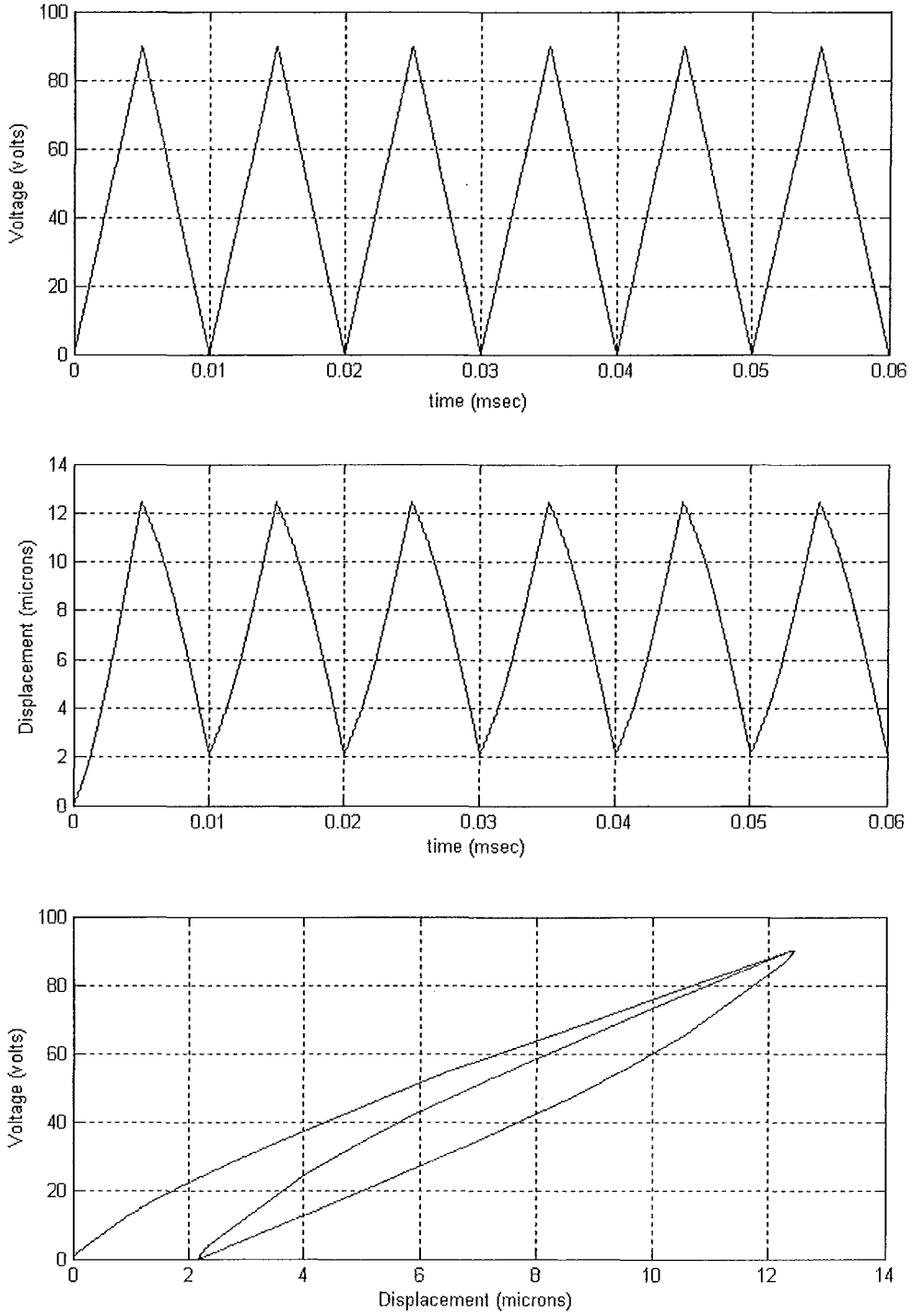

FIGURE 3.5: OUTPUT DISPLACEMENT AND VOLTAGE DISPLACEMENT BEHAVIOUR FOR A TEN ELASTO-SLIDE ELEMENT PZT ACTUATOR WITH A 90 VOLT TRIANGULAR INPUT VOLTAGE.

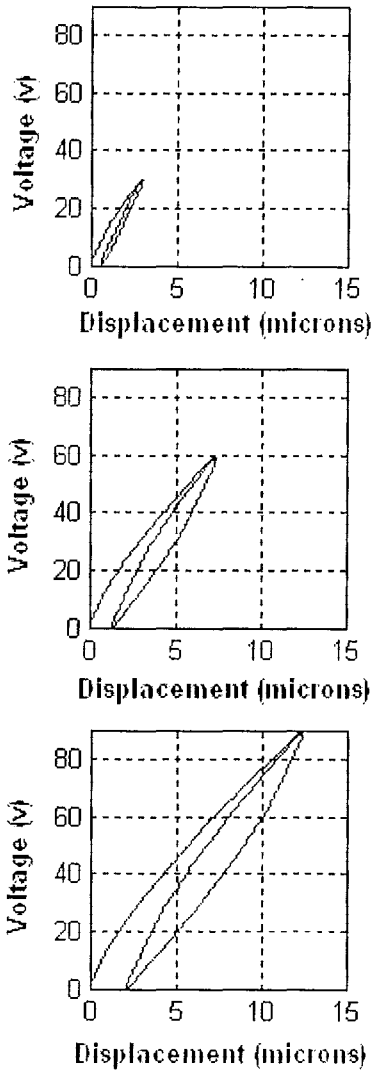

FIGURE 3.6: VOLTAGE DISPLACEMENT BEHAVIOUR FOR A TEN ELASTO-SLIDE ELEMENTS PZT ACTUATOR WITH 90, 60, AND 30 VOLT TRIANGULAR INPUT WAVEFORMS.

3.2.1 Closed loop PID control

The model is then enhanced to incorporate closed loop PID control of the PZT layer so that the PZT actuator can produce a desired input or reference displacement profiles. Optimum gain parameters are determined by trial and error. They are 39.5, 1.8, and 40.5 for proportional (P), differential (D), and integral (I) gains respectively. Simulations are done for a step input, a step input with external force, and a step input

with delayed external force applied after steady state has been reached. Results for these simulations are shown in Figures 3.7 to 3.9.

Figure 3.7 shows displacement behaviour for step inputs with varying reference displacements showing that the closed-loop, feedback controlled model is capable of tracking displacement profiles as small as 1 nm to a maximum of 12 μm. Figure 3.8 shows displacement behaviour for step inputs with an external force exerted on PZT actuator modelling a fixed mass. Figure 3.9 shows displacement behaviour for step response with an external force applied after steady state has been reached. Both Figures 3.8 and 3.9 show the stability of the model under such conditions, as well as the ability of the PZT layer to reach the commanded displacement using feedback control

Note also in each case that steady state is reached in 0.3 milliseconds or less. Hence, the system could be stepped at 3000 Hz or more with precision. However, to get greater displacement requires many layers, which traditionally lowers this peak actuation frequency.

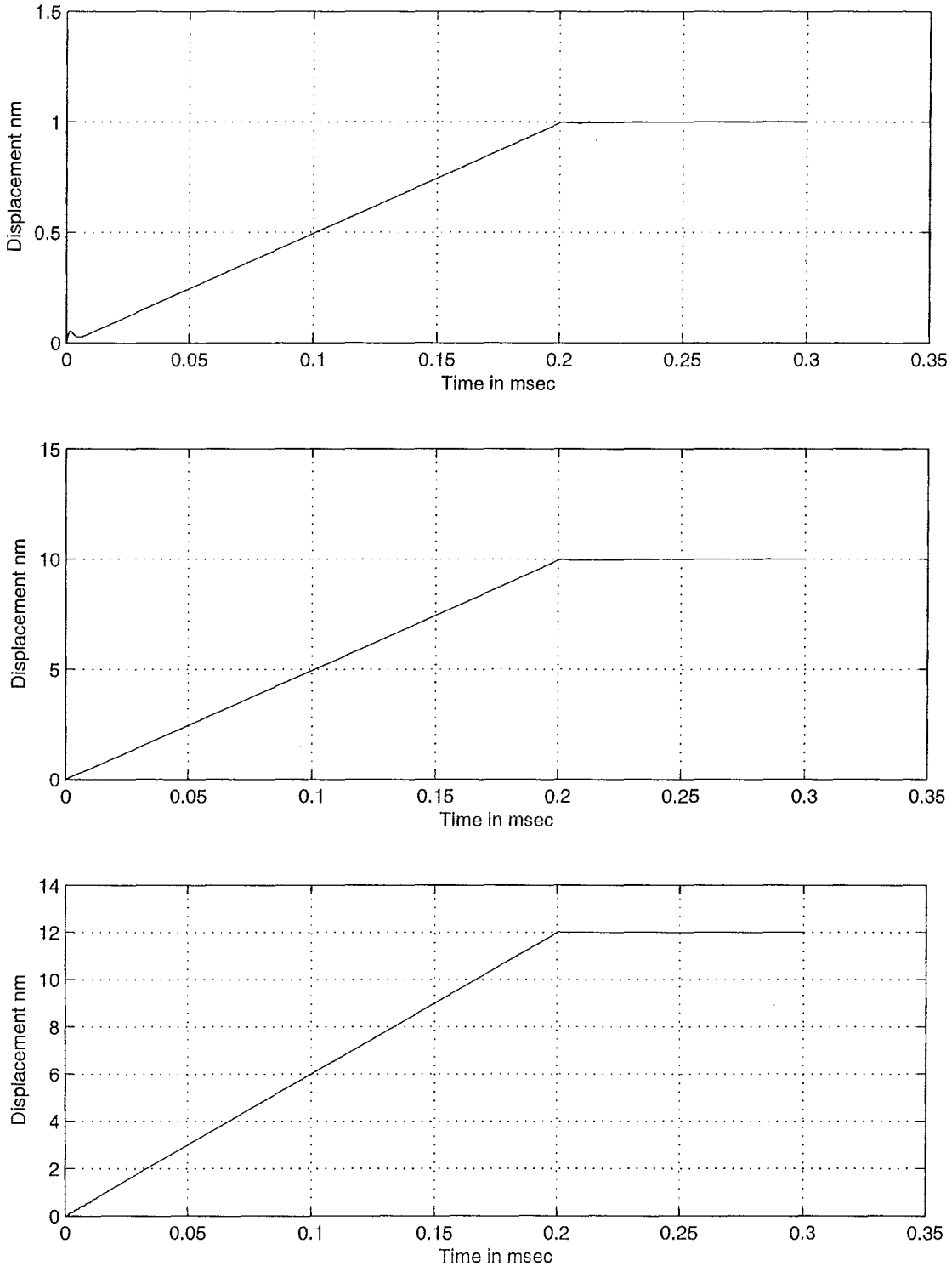

FIGURE 3.7: OUTPUT DISPLACEMENTS FOR DIFFERENT REFERENCE INPUTS SHOWING THE RANGE PZT ACTUATOR, FROM 1 NANOMETRE TO 12 MICROMETER.

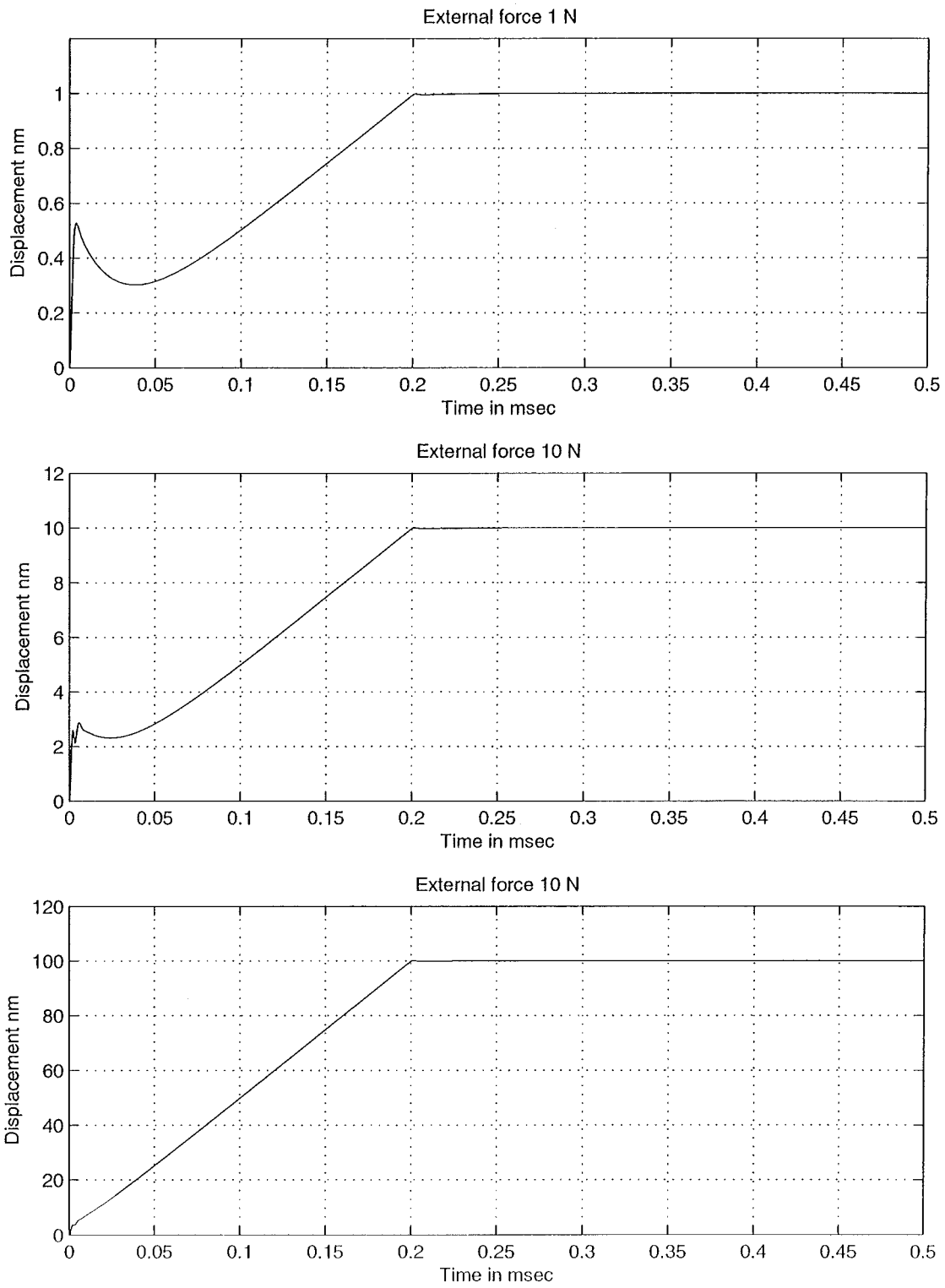

FIGURE 3.8: OUTPUT DISPLACEMENTS FOR DIFFERENT REFERENCE INPUTS WITH AN EXTERNAL FORCE OF 1 NEWTON

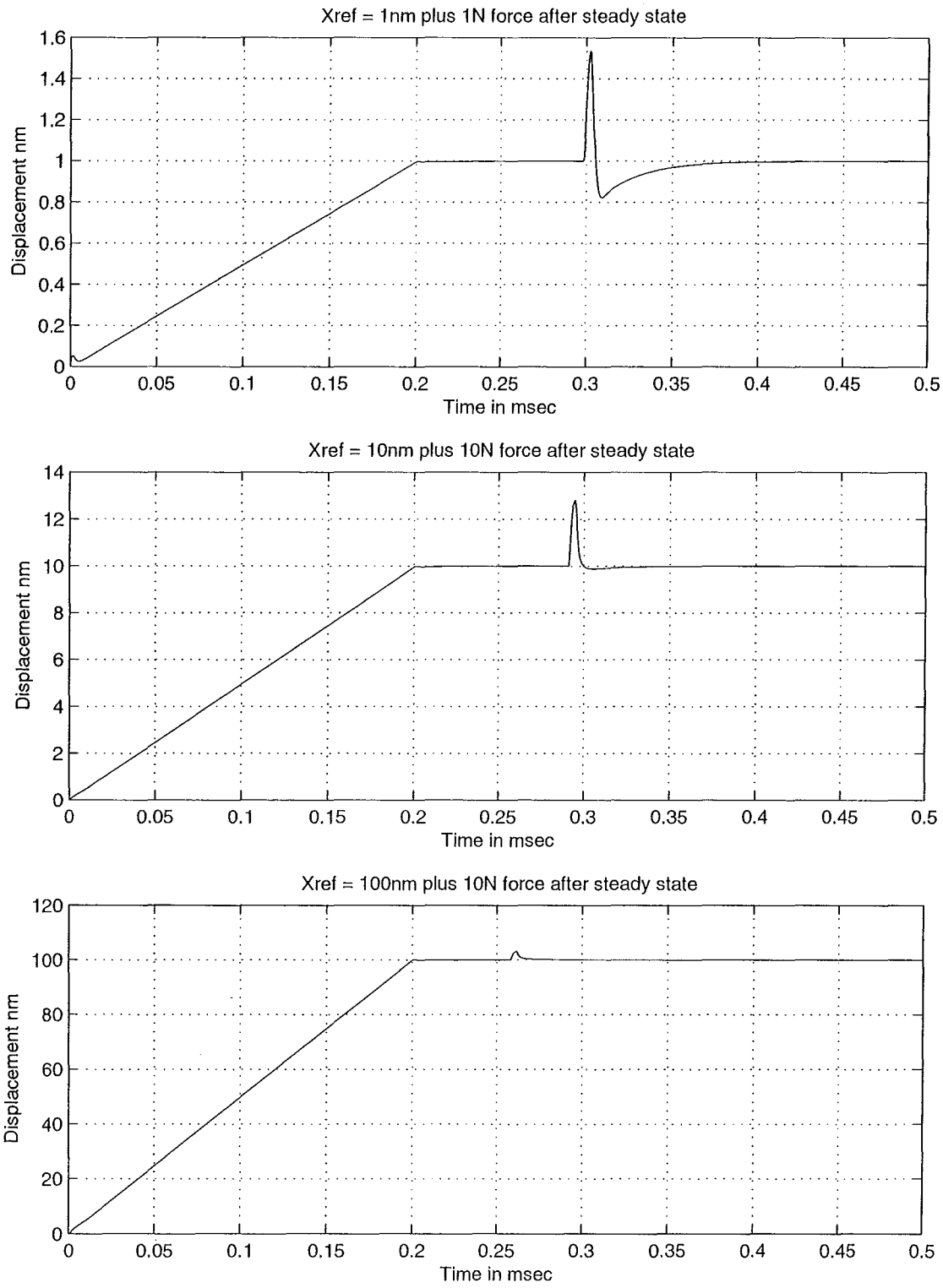

FIGURE 3.9: OUTPUT DISPLACEMENTS FOR DIFFERENT REFERENCE INPUTS WITH AN EXTERNAL FORCE APPLIED AFTER STEADY STATE.

3.3 Simplified Model (without the mass of PZT)

During the course of the simulations it was found that the model can be simplified by ignoring the mass of the PZT which is very small as shown in Table 2.2. One advantage of this approach is, that it requires for fewer integrations and computations to solve the problem. Figures 3.10 and 3.11 show comparisons done with the full model and the simplified model. These graphs illustrate that excluding the mass of the PZT does not affect model accuracy.

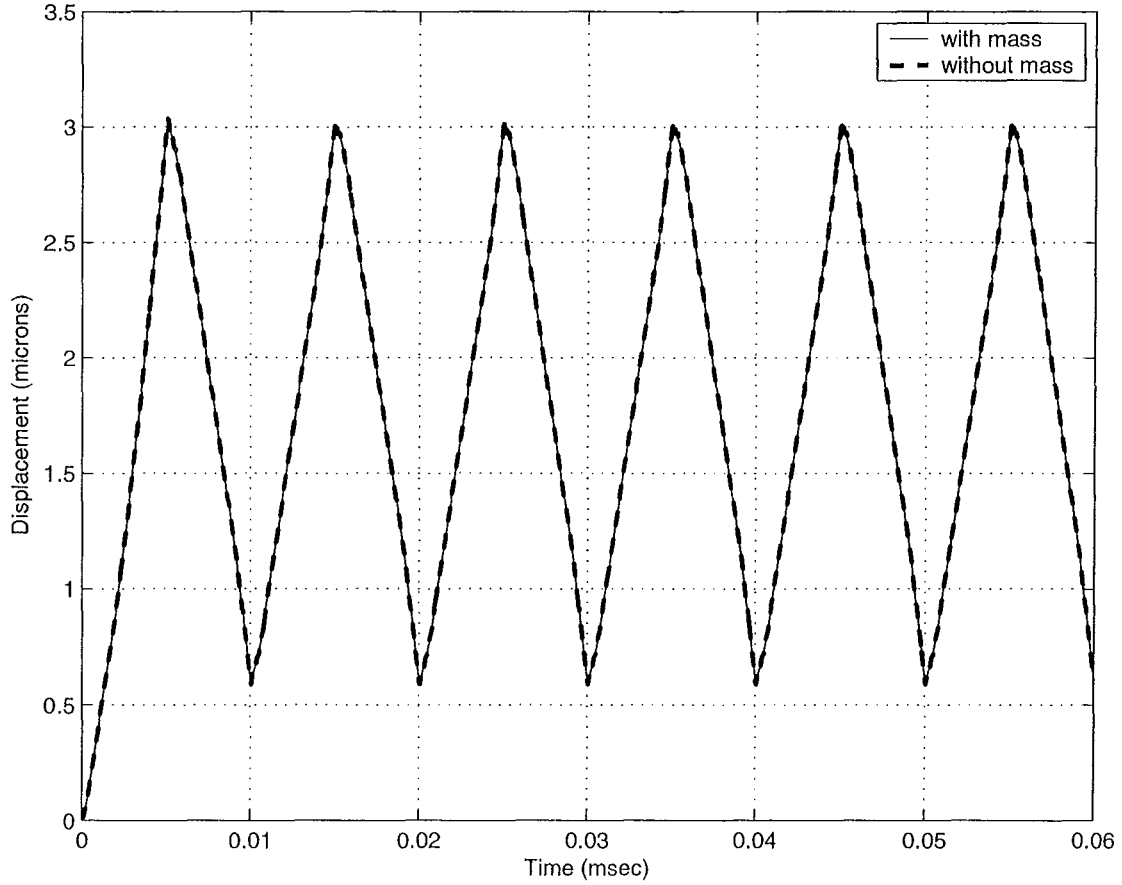

FIGURE 3.10: DISPLACEMENT BEHAVIOUR OF THE PZT FOR TRIANGULAR INPUT, FOR FULL MODEL (INCLUDING MASS OF PZT) AND SIMPLIFIED MODEL (EXCLUDING MASS).

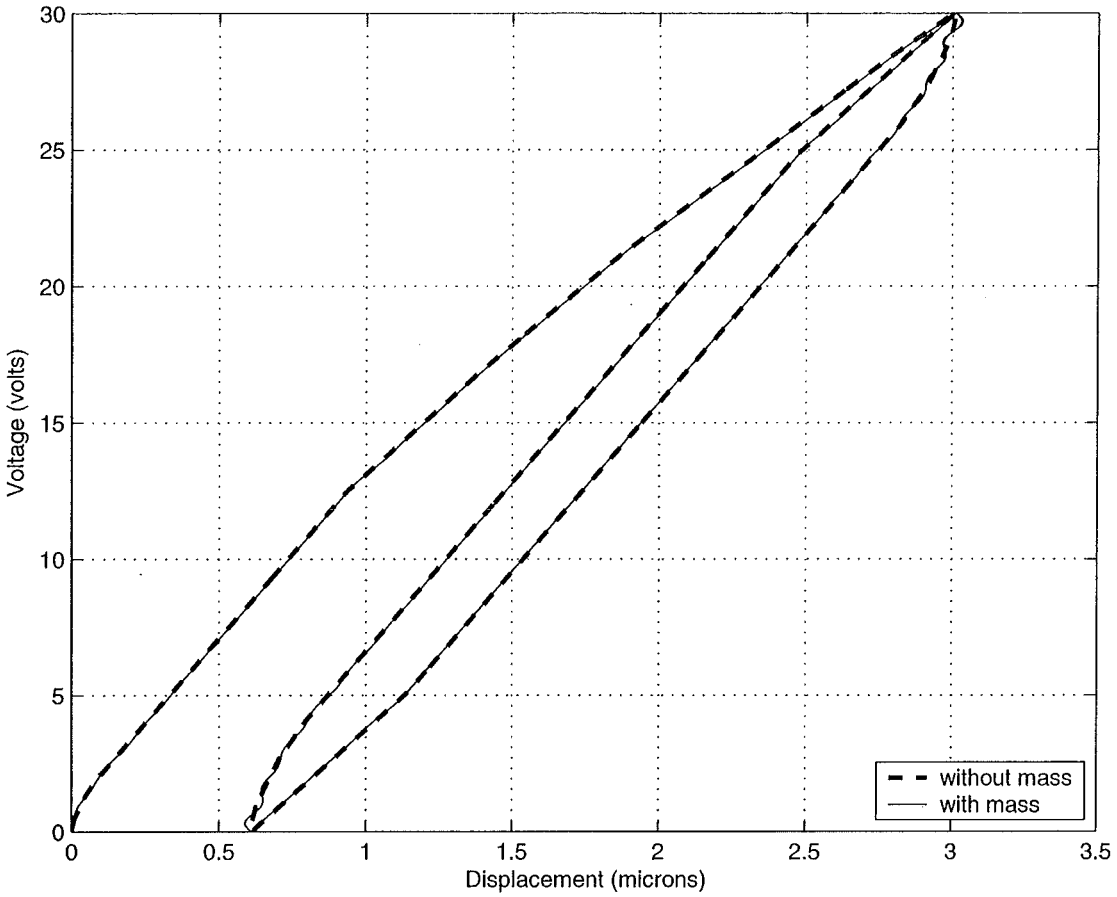

Figure 3.11: VOLTAGE VERSUS DISPLACEMENT BEHAVIOUR OF PZT ACTUATOR FOR TRIANGULAR INPUT, FOR FULL MODEL (INCLUDING MASS OF PZT) AND SIMPLIFIED MODEL (EXCLUDING MASS).

For this model, only Equation (1.6d) needs to be modified as follows:

$$bx' + kx = F_t + f_{ext} \tag{3.1}$$

The other equations that define this simplified model are Equations (1.6a), (1.6b), (1.6c), (1.6e), (2.4) and (2.6), which stays the same for this model.

The mean percentage difference error between the models with and without mass for the displacement response is 0.01% strengthening the decision to ignore the mass.

Chapter 4

4. Multi-Layer Analysis

A three layer PZT actuator is modelled by cascading three single layers in series as described in Chapter 2.3. The idea behind multilayer application is to control each layer independently to create a high stiffness, high frequency precision motion control actuator. This means that each layer must be separately activated while the other layers are held stiff. Three layers are used to demonstrate the concept, which can be extended to a greater number, as desired. The 3 layer model is shown schematically in Figure 4.1. Note that voltages can be independently applied to any, or all, layers.

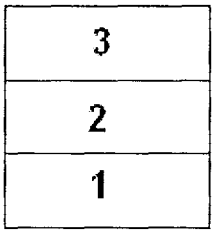

3 layer PZT actuator

FIGURE 4.1: SCHEMATIC MODEL OF A 3LAYER PZT ACTUATOR

4.1 Simulation of multilayer PZT actuator

First, triangular wave input voltage profiles are applied and the results are shown in Figures 4.1 to Figure 4.3. Figure 4.1 shows a triangular wave input voltage identically applied to all three layers simultaneously. When only layer 1 is activated displacements are still induced on layers 2 and 3. This behaviour is the result of forces interacting at the interface of two layers. Hence, if that added motion is undesired, it must be regulated using feedback control of the layers

The dynamics are more evident in Figure 4.2 where only layer 1 is activated with a 90 volt triangular wave, while 0 volts are applied to the other two layers. Here the induced displacements have larger effect on the adjacent layer. In this case layer 1 deflects to a maximum of 10.8 μm and layers 2 and 3 deflect to a maximum of 1 μm and 0.1 μm respectively. Note that layer 2 deflects more than layer 3 as the activated layer is closest to layer 2, and layer 3 only sees these interactions via the interactions of layer 2 with layer1.

This effect is clearly seen when layer 2 only is activated, as shown in Figure 4.3. In this case, the adjacent layers (1 and 2) have induced displacements of approximately 1 μm. Hence, with layer 2 actiavted, layers 2 and 3 see essentially equal interactions with the activated motion of layer2. Hence, their response is essentially identical.

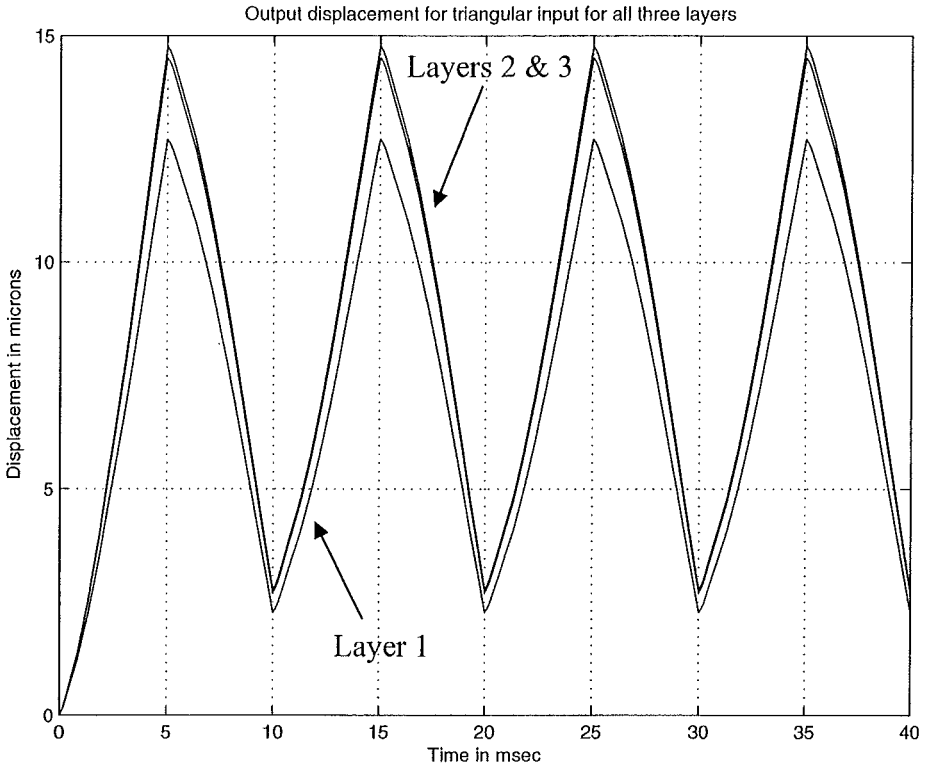

FIGURE 4.2: DISPLACEMENT BEHAVIOUR FOR 90 VOLT, 100 HERTZ, TRIANGULAR WAVE APPLIED TO ALL THREE LAYERS

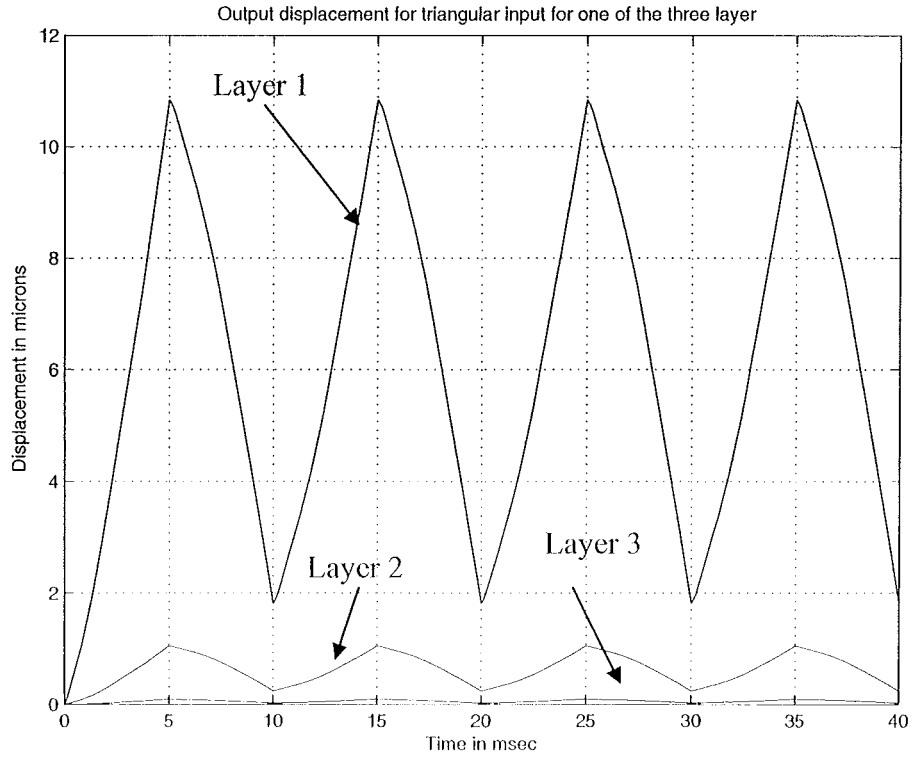

FIGURE 4.3: DISPLACEMENT BEHAVIOUR FOR ONLY LAYER 1 ACTIVATED

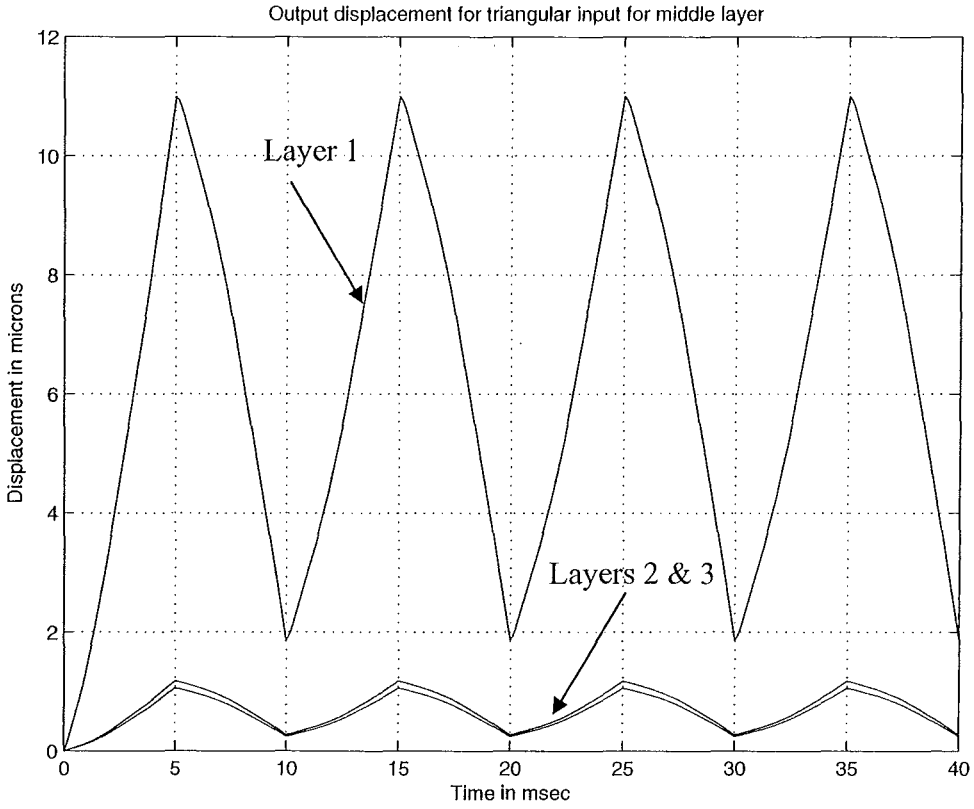

FIGURE 4.4: DISPLACEMENT BEHAVIOUR ONLY LAYER 2 ACTIVATED

Next, PID control is incorporated in the model so that the PZT actuator can produce desired displacement profiles. A different gain setting for the PZT layers is needed, compared to single layer alone, to get optimum output and is obtained by trial and error. The gain parameters used are P = 0.8, D = 10, and I = 10 for proportional, differential and integral gains respectively.

Initially, this closed-loop model is tested with step input applied to only one layer and the results are shown in Figures 4.4 to 4.7. These figures show displacement behaviour for varying input reference displacements of 1 nm to 12 μm, showing that the closed-loop, feedback controlled model is capable of tracking desired displacement profiles.

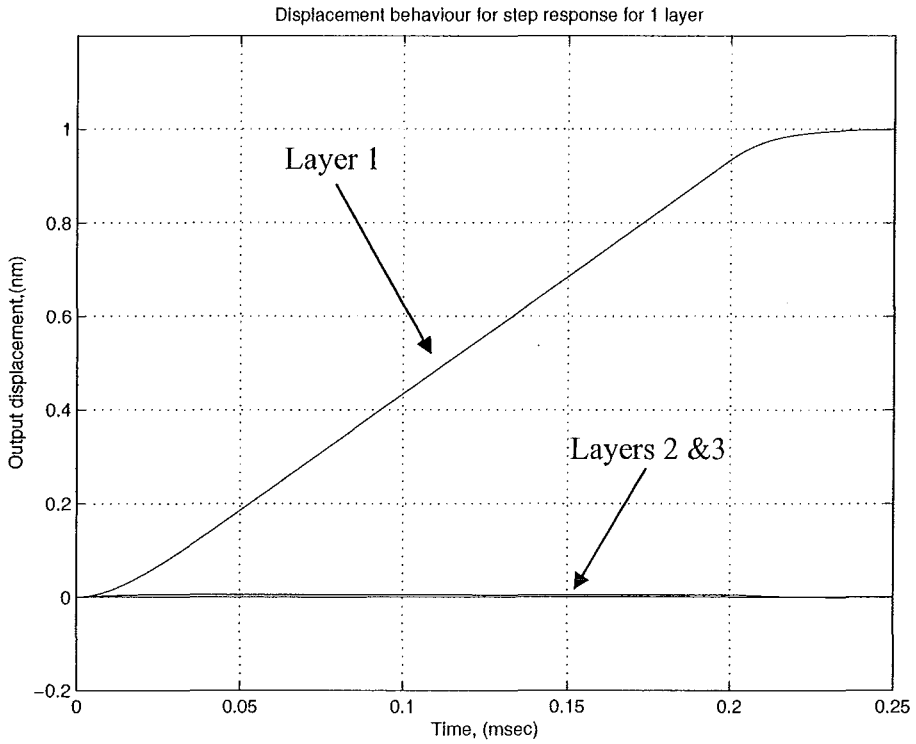

FIGURE 4.5: DISPLACEMENT BEHAVIOUR FOR 1 NANOMETRE REFERENCE INPUT

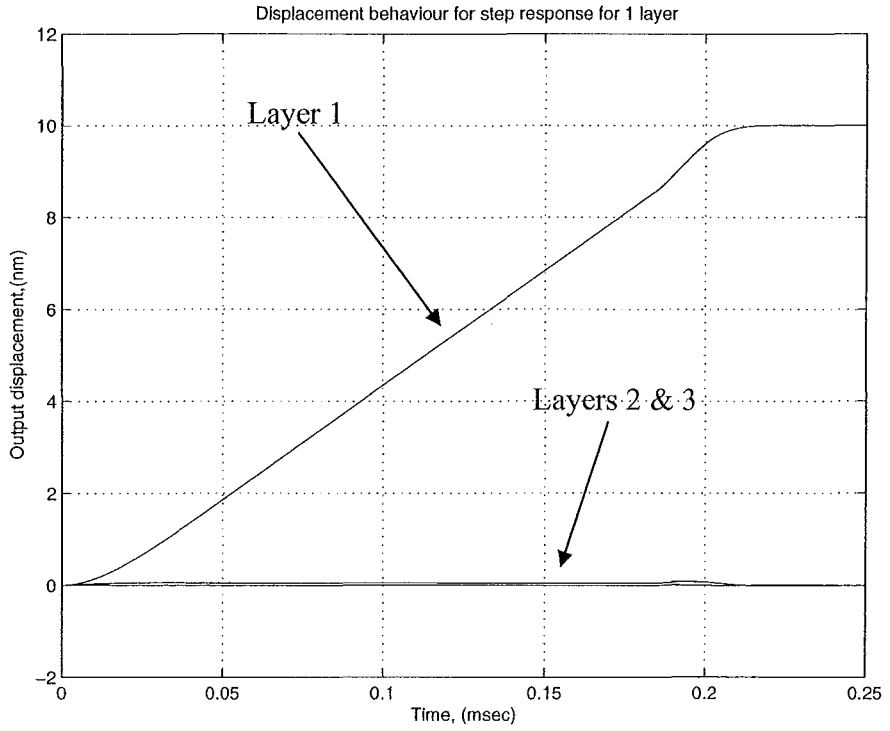

FIGURE 4.6: DISPLACEMENT BEHAVIOUR FOR 10 NANOMETRE REFERENCE INPUT

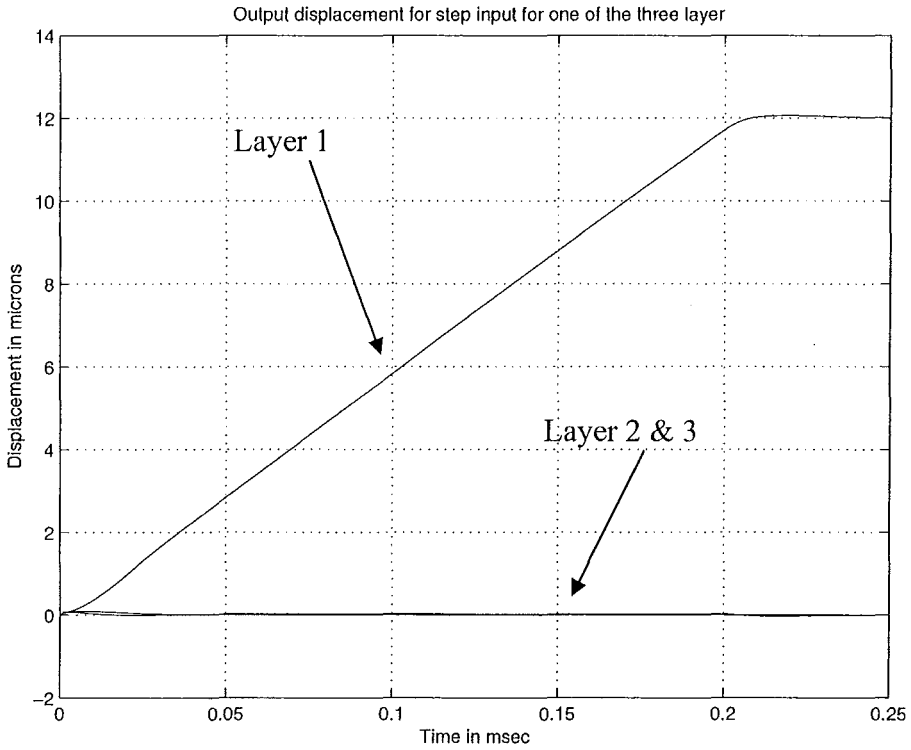

FIGURE 4.7: DISPLACEMENT BEHAVIOUR FOR 12 MICROMETRE REFERENCE INPUT

In each figure, the commanded displacement is obtained with in 0.25 milliseconds. In addition, the remaining two layers are controlled to 0 deflection, as desired. Hence, the PID controlled model is capable of moving and achieving displacements as small as 1 nm to 36 μm (if each layer is displaced by 12 μm) as commanded. Finally, in the first 0.1 to 0.5 milliseconds the other two layers (layers that are not activated), do undergo a deflection, yet are controlled to essentially 0 motion very rapidly.

Figure 4.8 shows reference input displacements of 1, 5 and 10 nm applied to layers 1, 2, and 3 respectively. It shows the ability of the PID controlled model to displace all three layers to a desired displacements simultaneously.

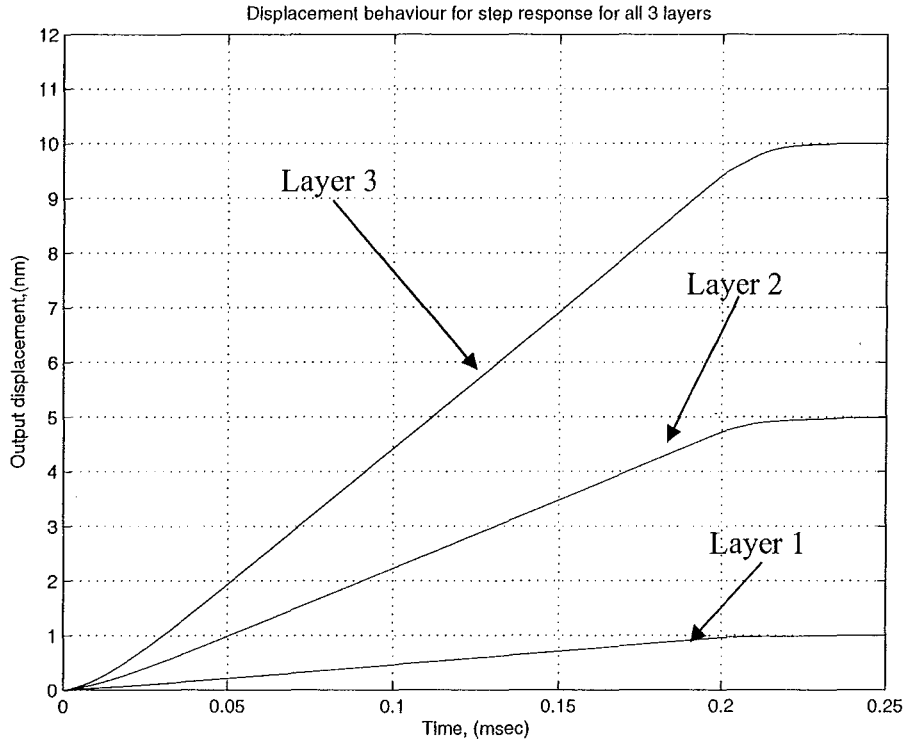

FIGURE 4.8: DISPLACEMENT BEHAVIOUR FOR 1, 5, AND 10 NANOMETRE REFERENCE INPUT APPLIED TO 3 LAYERS.

Finally, step input profiles, as shown in Figure 4.9 are applied to the PZT actuator, where a step input of 1 μm is applied for each layer, successively.

This creates a command input of 3 μm in distinct 1 μm steps. As such, it demonostrates the basic concept described in this thesis. First, a reference step input of 1 μm is applied to layer 1 while the other two layers are held at 0 displacement. Then a reference step input of 1 μm is applied to layer two while hold layer 1 at 1 μm and layer three at 0 displacements. Finally a reference step input of 1 μm is applied to layer three with layers 1 and 2 now held at 1 μm each, giving a total of 3 μm total displacement for the PZT actuator.

The end point output displacement behaviour for PZT is shown in Figure 4.10. Note that the desired displacements are achieved for each layer with in 0.25 milliseconds, showing the ability of the PZT actuator to reach commanded displacements. Since steady state is reached with in 0.25 milliseconds, or less, this system could be easily commanded at 3 – 4 kHz. Equally importantly, this command rate could be increased as needed to same extent. Note also that in Chapter 3, 1 layer had similar response times to the 3 layer model here, indicating that the PID control of each layer has maintained device stiffness, as desired.

Similar results to Figure 4.10 are shown in Figure 4.11 for 1 nm steps, showing the potential for much smaller motions and nano-lithography applications

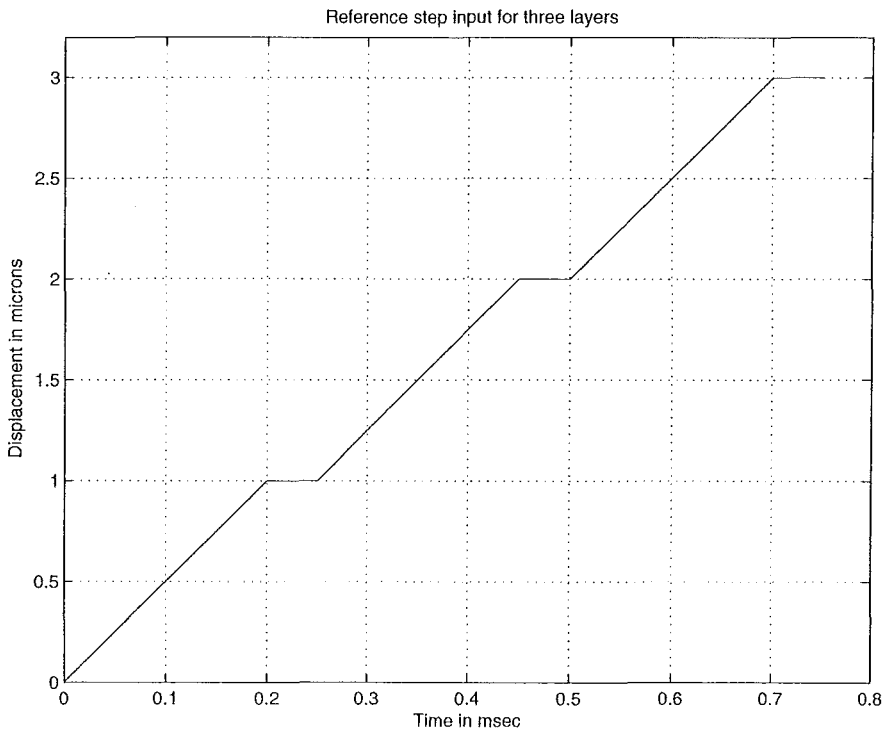

FIGURE 4.9: INPUT DISPLACEMENT COMMAND PROFILE FOR THREE LAYER ACTUATION

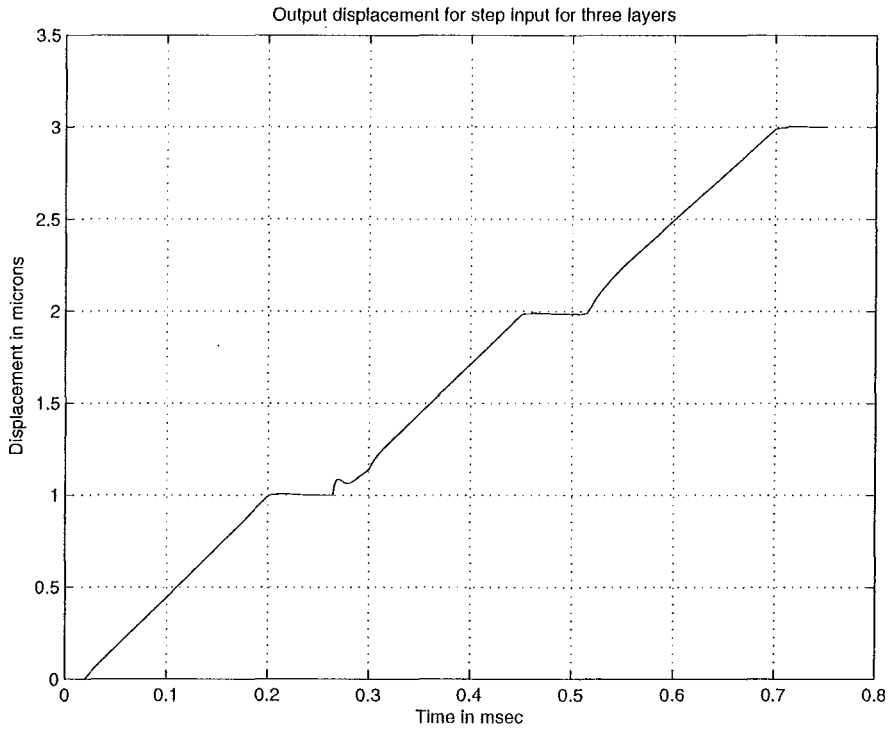

FIGURE 4.10: END POINT OUTPUT DISPLACEMENT BEHAVIOUR OF PZT ACTUATOR FOR INPUT DISPLACEMENT PROFILE SHOWN FIGURE 4.9

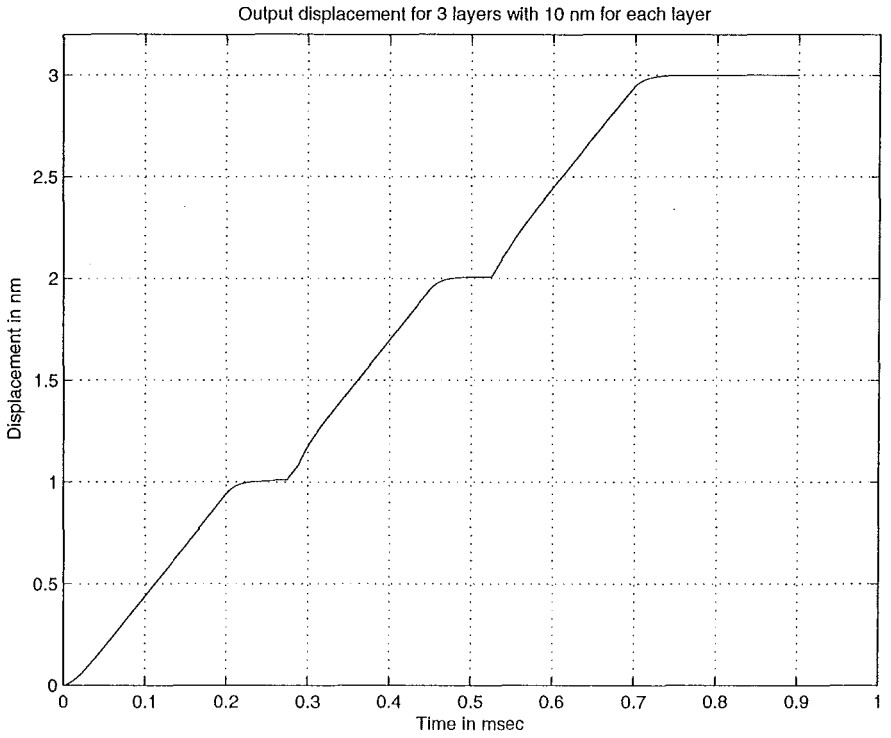

FIGURE 4.11: END POINT OUTPUT DISPLACEMENT BEHAVIOUR OF PZT ACTUATOR WITH 1NM STEP INPUTS AT EACH LAYER

The results show for even greater total actuator displacement, or "throw", more layers have to be added. However, the results in this chapter prove the essential concept for a number of displacements, and can be readily generalised to a larger number of layers

A major result worth noting again is the very short, 0.2-0.3 millisecond times to steady state for the commanded displacements. This result for the 3 layer model matches the single layer results despite the use of 3 springs in series instead of just 1. Normally, such a PZT stack would have an approximately 40-45% reduction in dynamic stiffness and an equal reduction in response time. Hence, controlling each layer individually enabled the system to maintain a higher dynamic stiffness, as desired. As a result, high frequency, high precision applications, like the MEMs-based e-beam lithography of Chase and Smith [6] rae now feasible at 3 kHz or greater driving frequencies

Chapter 5

5. Conclusions and Future Work

A model for a PZT actuator is developed based on work of Goldfarb and Celanovic [3], to capture both linear dynamics as well as the nonlinear effects of the electro-mechanical hysteresis. The model is developed in two stages. First, a single layer model is developed. Next it is generalised to a multi-layer model. PID control is implemented at each step using closed-loop feedback control to achieve desired displacement outputs. Both single layer model and multi-layer model are tested with different input profiles, to show the capability of this unique, individually actuated PZT layer approach to PZT stack actuation.

A single layer PZT model utilising PID feedback control showed the ability to reach commanded displacements for varying reference inputs from 1 nm to 12 μm. These displacements represent a range of possible applications from micro-surgery (10 μm) to nano-lithography (1-10 nm). The model was also tested for the influence of external forces and showed stability under such conditions, retaining the commanded displacement. For each case steady state is achieved in 0.3 milliseconds or less indicating the ability to drive the PZT actuator, with precision, and over 3 kHz..

A 3-element multi-layer PZT model extends this concept simply and directly showing the ability to respond to commanded displacement profiles from 1 nm – 36 μm representing a broad range of applications. Independent layer control is achieved using the PID control for each layer with closed-loop feedback of the reference input error, In each case the system was able to achieve commanded displacements to within 0.1%. This goal was achieved whether driving individual layers or all 3 layers in various sequences. Results were not affected by external forces or inter-layer interactions and reaction forces. All displacements were reached within 0.3 milliseconds indicating that high stiffness was maintained despite tripling the number of layers.

Experimental verification of the PZT model developed in Chapter 4 is required before it can be practically implemented. This will require repeating the results of Chapter 3 for a single layer first. Once verified, a multi-layer experimental model should be developed and tested. Of particular interest should be the influence or existence of any electrical field or capacitive "cross talk" between individually controlled layers. Also of interest will be the ability of power supply systems to drive the PZT at the necessary frequencies and amplitudes to achieve the performance shown.

References

1. Adriaens, J.M.T.A., de Koning, W.L., and Banning, R., "Modeling Piezoelectric Actuators", IEEE/ASME Transactions on Mechatronics, 2000, Vol. 5 no.4, pp. 331-41.

2. Ge, P. and Jouaneh, M., "Tracking Control of a Piezoceramic Actuator", IEEE Transactions on Control Systems Technology, 1996, Vol. 4 no.3, pp. 209-216.

3. Goldfarb, M. and Celonovic, N., "Modeling Piezoelectric Stack Actuators for Control of Micromanipulation", IEEE Control Systems Magazine, 1997, Vol. 17 no.3, pp. 69-79.

4. Kawakita, S., et al., "Multi-Layered Piezoelectric Bimorph Actuator", Proceedings of the 1997 International Symposium on Michromechanics and Human Sciences, 1997, Japan.

5. King, T., Pozzi, M., and Manara, A., "Piezoactuators for 'Real-World' Applications, Can They Deliver Sufficient Displacement?" Power Engineering Journal, 2000, Vol. 14 no.3, pp. 105-10.

6. Chase, J.G. and Smith, B.S., "Overview of Modern Lithography Techniques and a MEMS-Based Approach to High Throughput Rate Electron Beam Lithography", Intelligent Material Systems and Structures, 2001, Vol. 12, pp. 807-17.

7. Choi, G.S., Kim, H.S., and Choi, G.H., "A Study on Position Control of Piezoelectric Actuators", IEEE International Symposium on Industrial Electronics, 1997, Portugal.

8. Lambert, P., et al., "Design and Performances of a One-Degree-of-freedom Guided Nano-Actuator", Robotics and Computer Integrated Manufacturing, 2003, Vol. 19, pp. 89-98.

9 "Theory and Applications of Piezo Actuators and PZT NanoPositioning Systems", Physik Instrumente (PI), Karluche, Germany, http://www.physikinstrumente.com/tutorial

10. "Piezoelectric Bending Actuators: Bimorphs Catalogue", Piezomechanik GmBh, Müchen, http://www.piezomechanik.com

11. Newcomb, C.V. and Flinn, I., "Increasing the Linearity of Piezoelectric Ceramic Actuators", Electronics Letters, 1982, Vol. 18, no.11:pp.442-443.

12. Adriaens, J.M.T.A., de Koning, W.L., and Banning, R., "Design and Modeling of Piezo-Actuated Positioning Mechanism", Proceedings of the 36th Conference on Decision and Control, 1997, California.

13. Goldfarb, M. and Celonovic, N., "Behavioural Implication of Piezoelectric stack Actuators for Control of Micromanipulation", IEEE International Conference on Robotics and Automation, 1996, Minnesota.

14. Yamagat, Y. and Higuchi, T., "A Micropositioning Device for Precision Automatic Assembly usinf Impact Force of Piezoelectric Elements", IEEE International Conference on Robotics and Automation, 1995, Japan.

15. Kleindiek, S., Kim, H.S., and Chang, T.H.P., "Miniature Three-axis Micropositioner for Scanning Proximal Probe and Other Applications", Journal of Vacuum Science and Technology B, Vol. 13, no.6:pp.2653-56.

16. Lazan, B.J., "Damping of Members and Materials in Structured Mechanics", 1968, Pergomon Press, London.

Appendix

MATLAB codes for multilayer step input model

```
%main code to run the program
clear
global Iold

T0=0.005;
ttotal=0:0.25e-6:0.00025;
qmax=1.6e-4;
qi1=0; qbi1=zeros(1,10);
qi2=0; qbi2=zeros(1,10);
qi3=0; qbi3=zeros(1,10);
t_q=[0:1e-5:0.001,0.0011:1e-4:T0];
qqq1=qmax/T0*t_q;
qqq2=qmax/T0*t_q;
qqq3=qmax/T0*t_q;

Xref1=0; Xref2=0; Xref3=0;
err1=0; err2=0; err3=0;
Iold1=0; Iold2=0; Iold3=0;
Vold1=0; Vold2=0; Vold3=0;
Vnew1=1; Vnew2=1; Vnew3=1;
X=[0 0 0]; j=2
```

```
Xrfamp1=1e-9; Xrfamp2=5e-9; Xrfamp3=10e-9;


Xref1(j)=ppulse(ttotal(j),Xrfamp1);
Xref2(j)=ppulse(ttotal(j),Xrfamp2);
Xref3(j)=ppulse(ttotal(j),Xrfamp3);
X0=X(end,:);

err1(j)=Xref1(j)-X0(1);
err2(j)=Xref2(j)-X0(2);
err3(j)=Xref3(j)-X0(3);

Iold=Iold1;
errK1=applygains(err1,j,1e-5);
Iold1=Iold;

Iold=Iold2;
errK2=applygains(err2,j,1e-5);
Iold2=Iold;

Iold=Iold3;
errK3=applygains(err3,j,1e-5);
Iold3=Iold;

Vnew1=getV(errK1);
Vnew2=getV(errK2);
Vnew3=getV(errK3);
```

```
clear vrc1 vrc2 vrc3
qinew1=qi1; qbinew1=qbi1;
qinew2=qi2; qbinew2=qbi2;
qinew3=qi3; qbinew3=qbi3;

for i=2:length(qqq1)
   [vrc1(i),qi1,qbi1]=v_rc(qqq1(i),2,qi1,qbi1);
   [vrc2(i),qi2,qbi2]=v_rc(qqq2(i),2,qi2,qbi2);
   [vrc3(i),qi3,qbi3]=v_rc(qqq3(i),2,qi3,qbi3);
end
tspan=[ttotal(j-1) ttotal(j)];
q_vector1=qqq1; vrc_vector1=vrc1;
q_vector2=qqq2; vrc_vector2=vrc2;
q_vector3=qqq3; vrc_vector3=vrc3;
Vnew=[Vnew1 Vnew2 Vnew3]; Vold=[Vold1 Vold2 Vold3];
[TT,XX]=ode15s(@DE_system_actuator,tspan,X0,[],q_vector1,vrc_vector1,q_vector2,v
rc_vector2,q_vector3,vrc_vector3,Vnew,Vold);
X(j,:)=XX(end,:);


for j=3:length(ttotal)


[dx,q_final1,q_final2,q_final3]=DE_system_actuator(TT(end),X(end,:),q_vector1,vrc_v
ector1,q_vector2,vrc_vector2,q_vector3,vrc_vector3,Vnew,Vold);
   qi1=qinew1; qbi1=qbinew1;
   qi2=qinew2; qbi2=qbinew2;
   qi3=qinew3; qbi3=qbinew3;
```

```
[vrc1,qi1,qbi1]=v_rc(q_final1,2,qi1,qbi1);
[vrc1,qi1,qbi1]=v_rc(q_final1+(-1)^(i+1)*1e-12,2,qi1,qbi1);
[vrc2,qi2,qbi2]=v_rc(q_final2,2,qi2,qbi2);
[vrc2,qi2,qbi2]=v_rc(q_final2+(-1)^(i+1)*1e-12,2,qi2,qbi2);
[vrc3,qi3,qbi3]=v_rc(q_final3,2,qi3,qbi3);
[vrc3,qi3,qbi3]=v_rc(q_final3+(-1)^(i+1)*1e-12,2,qi3,qbi3);
t_q=[(i-1)*T0:1e-5:(i-1)*T0+0.001,(i-1)*T0+0.001+1e-4:1e-4:i*T0];
q0_1=q_final1;
q0_2=q_final2;
q0_3=q_final3;
if round(i/2)==i/2
   q1_1=0;
   q1_2=0;
   q1_3=0;
else
   q1_1=qmax;
   q1_2=qmax;
   q1_3=qmax;
end
qqq1=q0_1+(q1_1-q0_1)/T0*(t_q-(i-1)*T0);
qqq2=q0_2+(q1_2-q0_2)/T0*(t_q-(i-1)*T0);
qqq3=q0_3+(q1_3-q0_3)/T0*(t_q-(i-1)*T0);

Vold1=Vnew1;
Vold2=Vnew2;
Vold3=Vnew3;

Xref1(j)=ppulse(ttotal(j),Xrfamp1);
```

```
Xref2(j)=ppulse(ttotal(j),Xrfamp2);
Xref3(j)=ppulse(ttotal(j),Xrfamp3);
X0=X(end,:);

err1(j)=Xref1(j)-X0(1);
err2(j)=Xref2(j)-X0(2);
err3(j)=Xref3(j)-X0(3);

Iold=Iold1;
errK1=applygains(err1,j,1e-5);
Iold1=Iold;

Iold=Iold2;
errK2=applygains(err2,j,1e-5);
Iold2=Iold;

Iold=Iold3;
errK3=applygains(err3,j,1e-5);
Iold3=Iold;

Vnew1=getV(errK1);
Vnew2=getV(errK2);
Vnew3=getV(errK3);

clear vrc1 vrc2 vrc3
qinew1=qi1; qbinew1=qbi1;
qinew2=qi2; qbinew2=qbi2;
qinew3=qi3; qbinew3=qbi3;
for ii=1:length(qqq1)
```

```
    [vrc1(ii),qi1,qbi1]=v_rc(qqq1(ii),2,qi1,qbi1);
    [vrc2(ii),qi2,qbi2]=v_rc(qqq2(ii),2,qi2,qbi2);
    [vrc3(ii),qi3,qbi3]=v_rc(qqq3(ii),2,qi3,qbi3);
  end


  q_vector1=qqq1; vrc_vector1=vrc1;
  q_vector2=qqq2; vrc_vector2=vrc2;
  q_vector3=qqq3; vrc_vector3=vrc3;

  tspan=[ttotal(j-1) ttotal(j)];
  Vnew=[Vnew1 Vnew2 Vnew3]; Vold=[Vold1 Vold2 Vold3];

[TT,XX]=ode15s(@DE_system_actuator,tspan,X0,[],q_vector1,vrc_vector1,q_vector2,v
rc_vector2,q_vector3,vrc_vector3,Vnew,Vold);
  X(j,:)=XX(end,:);

end

figure(1); plot(ttotal,X*1e6);

%function that defines the actuator
function
[dx,q1,q2,q3]=DE_system_actuator(t,x,q_vector1,vrc_vector1,q_vector2,vrc_vector2,q
_vector3,vrc_vector3,Vnew,Vold)

k=6e6; b=150; C=1.2e-6; T=10;
```

```
vin1=ppulse(t,Vnew(1),Vold(1));
vin2=ppulse(t,Vnew(2),Vold(2));
vin3=ppulse(t,Vnew(3),Vold(3));

vrc1=fzero(@q_solve,0,optimset('TolX',1e-
12,'Display','off'),vin1,x(1),q_vector1,vrc_vector1);
vrc2=fzero(@q_solve,0,optimset('TolX',1e-
12,'Display','off'),vin2,x(2),q_vector2,vrc_vector2);
vrc3=fzero(@q_solve,0,optimset('TolX',1e-
12,'Display','off'),vin3,x(3),q_vector3,vrc_vector3);

q1=T*x(1)+C*(vin1+vrc1);
q2=T*x(2)+C*(vin2+vrc2);
q3=T*x(3)+C*(vin3+vrc3);

F1t=T*(vin1+vrc1);
F2t=T*(vin2+vrc2);
F3t=T*(vin3+vrc3);

dx=[-k/b*x(1)+1/b*(F1t+F2t+F3t);          -k/b*x(2)+1/b*(F1t+2*F2t+2*F3t);          -
k/b*x(3)+1/b*(F1t+2*F2t+3*F3t)];


%function to apply gains


function errK=applygains(err,i,stp)
global Iold

%set gains
```

```
KP=0.8; KD=10e-6; KI=10000;

Inew=KI*stp*err(i) + Iold;
D=(err(i)-err(i-1))*KD/stp;

S=D+Inew+err(i);


errK=KP*S;

Iold=Inew;



%function to get the voltages

function amp=getV(err)

err=err*1e6;

if err==0
   amp=0;
else
   amp=-0.263*err^2 + 10.939*err;
end



%function to get the input profiles
function vin = ppulse(t,Vnew,varargin)

%set risetime
R=0.2e-3;


switch nargin,
   case 2;
      Vold=0;
      Vf=0;
      m=abs(Vold-Vnew)/R;
```

```
    if Vnew>Vold
      if t<R
        vin=Vold + 1*m*t;
      else
        vin=Vnew;
      end
    else
      if t<R
        vin=Vold - 1*m*t;
      else
        vin=Vnew;
      end
    end

  case 3;
    Vold=varargin{1};
    Vf=0;
    m=abs(Vold-Vnew)/R;

    if Vnew>Vold
      if t<R
        vin=Vold + 1*m*t;
      else
        vin=Vnew;
      end
    else
      if t<R
        vin=Vold - 1*m*t;
      else
        vin=Vnew;
      end
    end


  case 4;
    Vold=varargin{1};
    Vf=varargin{2};
    m=abs(Vold-Vnew)/R;

    if Vnew>Vold
      if t<R & Vold<=Vf*0.999
        vin=Vold + 1*m*t;
```

```
        else
          vin=Vnew;
        end
      else
        if t<R & Vold<=Vf*0.999
          vin=Vold - 1*m*t;
        else
          vin=Vnew;
        end
      end

end



%function to solve for charge, q
function qq=q_solve(vrc,vin,x,q_vector,vrc_vector)

%the equation q=T*x+C*(vin+vrc(q))

T=10; C=1.2*1e-6;

qq=interp1(vrc_vector,q_vector,vrc,'linear','extrap')-(T*x+C*(vin+vrc));


%function to calculation vrc
function [vrc,qi,qbi]=v_rc(q,n,qi,qbi)

q=q*1e6;

%global qi qbi

qinew=qi;
qbinew=qbi;

k=[2,0.6,0.3,0.26,0.06,0.1,0.05,0.03,0.1,0.5];

v=[0.2,0.3,0.3,2.6,0.9,2.0,1.5,1.2,7.0,80.0];

for i=1:10
   V1=k(i)*(q-qbi(i));
   if abs(V1)<v(i)
      V(i)=V1;
```

```
    else
        V(i)=v(i)*sign(q-qi);
        qbi(i)=q-v(i)*sign(q-qi)/k(i);
    end
end
qi=q;

%only update qi and qbi after each step of Euler's method as during the
%solving of q=T*x+C*(vin+vrc(q)), qi and qbi must be held at the same
%values, hence in this case the command v_rc(q,2) is used, otherwise the
%command v_rc(q,1) is used.
if n==1
    qi=qinew;
    qbi=qbinew;
end

%note the minus sign
vrc=-sum(V);
```